Simulations of the Dynamics Generated by Solar Global Oscillating Eigenmodes Generated in the Solar Atmosphere

M.K.Griffiths[a,b,*], V.Fedun[c], R.Erdélyi[a]

[a] *Solar Physics and Space Plasma Research Centre (SP^{2}RC), School of Mathematics and Statistics, University of Sheffield, Hicks Building, Hounsfield Road, S7 3RH, UK*
[b] *Corporate Information and Computing Services, The University of Sheffield, 10-12 Brunswick Street, Sheffield, S10 2FN, UK*
[c] *Department of Automatic Control and Systems Engineering, The University of Sheffield, Mappin Street, Sheffield, S1 3JD, UK*

Abstract

The solar atmosphere exhibits a diverse range of wave phenomena one of the earliest to be discovered was the five minute oscillation, the p-mode. The solar p modes are generated by global resonant oscillations and turbulent motions just beneath the photosphere. The resulting propagation of this wave energy into the solar atmosphere may be used as a diagnostic tool to predict some of the physical characteristics of the suns atmospheric layers.Report a study of synthetic photospheric oscillations in both non magentic and magnetic model of the quiet sun

The objective of this paper is to investigate the dynamics in the solar atmosphere which are generated by solar global eigenmodes of oscillation and to understand mechanisms of leakage of 5 min global oscillations into the atmosphere. Understand the conditions under which chromospheric dynamics evolve as a result of the 5 minute global oscillations - (spicules, waves). The main idea of performed simulations is to understand how energy supplied by various wave modes (the supplied energy is same for all of them) is redistributed in the atmosphere. Establish a link between signals at the photospheric levels and those at Coronal levels and shed light on the mechanisms leading to ubiquitous intensity oscillations in the solar atmosphere. The drivers in these simulations are different from our previous numerical experiments i.e. here we perturbed the whole bottom boundary.

We report on a series of hydrodynamicsl simulations modelling a realistic solar atmosphere using a driver located at 0.5Mm above the temperature minimum. With the objective of recreating atmospheric motions generated by global resonant oscillation the driver is spatially structured and is extended in a sinusoidal profile arcoss the base of the computational model. To carry out the simulations, we employed our the MHD code SMAUG (Sheffield MHD Accelerated Using GPUs). A combination of the VALIIIC and McWhirter solar atmospheres and coronal density profiles were used as the background equilibrium model in the simulations. Vertical and horizontal harmonic sources, located at the footpoint region of the open magnetic flux tube, are incorporated in the calculations, to excite oscillations in the domain of interest.

Our results demonstrate the conversion of modes with a period of 30s to a mode with a period of 180s, demonstrating that the Chromosphere is a source of 180s modes. The results inidicate a shift in frequency arising from interference between the driven waves

and reflections from the transition layer.

Keywords: magnetohydrodynamics (MHD); oscillations; MHD waves; solar atmosphere

1. Introduction

The solar atmosphere exhibits a diverse range of wave phenomena. The first Observations of oscillatory behaviour reported vertical motions on the solar surface with an amplitude of 300-400m/s with a period of 296s observations of Ca K band [1]. These ubiquitous oscillations are referred to as the p-modes. These motions were attributed to standing acoustic waves in the solar interior [2]. It was reported that the vertical wavelength is comparable to the horizontal wavelength and is roughly 1000-5000km [3]. The main restoring force for these modes of oscillation is the pressure, the 5 minute oscillation is the main manifestation of these modes. The solar p modes are generated by global resonant oscillations, periodic and turbulent motions just beneath the photosphere. These resonant modes are reflected at the surface by the steep change in density. The increase of the sound speed causes refraction. The resulting propagation of this wave energy into the solar atmosphere may be used as a diagnostic tool to predict the physical characteristics of the suns atmospheric layers. We report on a series of hydrodynamical simulations modelling a realistic solar atmosphere using a driver located at the temperature minimum, the driver is extended in a sinusoidal profile arcoss the base of the computational model. The objectives of this work is to recreate the atmospheric motions generated by the global resonant oscillation, to understand how the energy provided by different modes of oscillation are redistributed in the solar atmosphere and to shed light on the mechanisms which lead to ubiquitous intensity oscillations in the solar atmosphere.

2. Observations and Computational Studies Oscillations in the Solar Atmosphere

There is a significant body of work reporting on observational, theoretical and computational studies of p-mode phenomena. This work generally describes mechanisms for the propagation of energy into the Chromosphere, into the Solar Corona or between the transition region and the Corona. We briefly summarise some of this work here.

The energy sources heating both the Chromosphere and the Corona are still undetermined different thermo-mechanical or magnetic processes may contribute, particularly unclear is the quantity of power required to maintain chromospheric and coronal temperatures. The VALIIIC model of [4] is characterised by a total heat flux of $14000W/m^2$, 90% of this is dissipated near the base of the temperature plateau of the solar atmosphere the measurements suggest radiative losses of around $4300W/m^2$.

*Corresponding author at: Corporate Information and Computing Services, The University of Sheffield, 10-12 Brunswick Street, Sheffield, S10 2FN, UK. e-mail address: m.griffiths@sheffield.ac.uk

The growing field of coronal seismology uses the observed solar atmospheric wave modes to determine the physical characterisitcs of the solar atmosphere. This in turn requires a thorough understanding of the physics of the solar atmosphere. Although there is overwhelming evidence for photospheric 5 minute p-modes and 3 minute Chromospheric modes, the detection of oscillatory in the corona are rare and difficult to detect, making the solution of the coronalheating problem more challenging. However, since the advent of Coronal Seismology [5] [6] many spaced based high resolution systems (SOHO, TRACE, SDO) have provided evidence for wave like perturbations in the solar atmosphere. The work of [**?**] provides a detailed study of intensity oscillations in the solar atmosphere. Using SDO/AIA data they study image sequences at somlar minimum and maximum for diffrent solar regions e.g. active regions, quiet sun and a coronal hole. They consider a lower coronal channel, hot coronal channel and a cooler coronal channel. The study revealed strong 3-5 minute oscillations in all channels and included some longer period modes. The results indicated that diffrences my arise when the size of the area of observation is changed.The ubiquity of the observed 3 and 5 minute oscillations in all channels and regions is an indication of a global excitation mechanism.

Imagery from SDO 171$\mathring{A}$ and 193$\mathring{A}$ was used by [**?**] to compute the Fourier power spectra in the Corona. Studying four regions of the solar atmosphere with different characteristics, they found that the distribution obeys a power law at low frequencies and possesses a flat distribution at high frequencies. This contrasts with the idea of a Gaussian noise distribution and a long time scale background. The implication is that this is the result of solar atmospheric heating from everywhere by small energy deposition events. It is expected that further measurements will constrain computational models.

Evidence for the upward propagation of acoustic wave with increasing amplitude has been demonstrated through a studies of variation in the intensities of Chromospheric lines for example the Ca lines at 854nm [7]. Although the observed variations are unlikely to provide temperature rises observed in the Chromosphere they are a clear indication of the increase in dynamical activity from the photosphere to the chromosphere. Using Fourier and wavelet analysis of time sequences from the Observatorio del Teide/Tenerife with the Gottingen Fabry-Perot interferometer [**?**] find that at a height of 250km there is an acoustic energy flux of $3000W/m^2$ 2/3 of this energy is propagated by waves in the frequency range 5-10mHz, the remaining third is carried by waves in the frequency range 10-20mHz. Waves with frequencies greater than the acoustic cut-off of 190s can contribute to the heating of the solar chromosphere. Reporting on measurements from the the Fe I 5434$\mathring{A}$ [**?**] detect waves with periods down to $40s$. For periods below the cutoff of $190s$ 40

[8] studied the upward propagation of acoustic shocks in the solar chromosphere they used a 1D computational model with a realistic model of the solar atmosphere and a model of radiative transfer. The resulting models of the generation of CaK2V bright points from acoustic waves with periods of 30, 180, and 300 s demonstrated that a 180s periodic driver produced results consistent with observations.

The question of Chromospheric heating by high frequency acoustic modes was addressed by Carlsson et al[**?**]. Using observational results from Hinode it was demonstrated that the energy flux due to acoustic modes in the frequency range 5-40mHz is less than $800W/m^2$, this does not balance radiation losses in the Chromosphere by a factor of 5. It had been suggested that these acoustic modes can steepen and dissipate as Chromospheric shocks. A major uncertainty with high frequency power is related to

the spatial resolution. Studying the influence of magnetic structures, Vecchio et al 2008 [9] used IBIS imaging data to identify the spatio-temporal occurrence of the acoustic shocks and compared with photospheric dynamics by means of both Fourier and wavelet analysis. A non-linear steepening of waves propagating from the photosphere with periods below 180s. The maximum velocity observed was in the range $6 - 7km/s$. Their observations demonstrated that portions of the internetwork regions undergo very few shocks, as "shadowed" by the horizontal component of the magnetic field. This latter observation was revealed through the presence of chromospheric fibrils, observed in the core of the CaII line as slanted structures with distinct dynamical properties. The shadow mechanism appears to operate also on the very small scales of inter-network magnetic elements, and provides for a very pervasive influence of the magnetic field even in the quietest region analyzed.

Using the IMAX instrument on the sunrise observatory, Roth et al [**?**] reported evidence for the excitation of solar acoustic oscillations excited by turbulent flows in the dark intergranular lanes. Individual sunquakes with epicenters near the solar surface and located in the intergranular lanes, are assumed to feed continuously energy into the resonant p-modes of the Sun and provide sources for acoustic oscillations. Roth presents wavefronts rippling near a granule and oriented along the direction of the intergranular lane. Using simultaneous observations of the Na and K lines with Doppler measurements Jefferies et al [10] show that inclined magnetic field lines provide portals along which magnetoacoustic energy can propaget at the inetrgranualr boundaries.

Sunspot oscillations have been detected unambiguously since the 1970s but there remain many questions regarding their generation mechanism, for example the connection between the 5-minute global p modes and the 5 minute modes in the photosphere [11]. A review of oscillations in sunspots was undertaken by [**?**]. The study identifies the importance of mode mixing and transformation also discussed is the generation of 3 minute modes resulting from the amplitude steepening of photospheric p-modes above the cutoff [12]. Energy from acoustic p-modes is converted to MHD modes and propagates along magnetic field lines in the pores. Observational evidence indicates the importance of high resolution studies for revealing the behaviour of acoustic energy flux in the solar atmosphere. [**?**] use high resolution data from the IMaX/Sunrise telescope to demonstrate that acoustic flux power, with periodsgreater than 100s carry at least half of the flux required to balance observed radiative losses in the solar Chromosphere. The main contrivution to theis flux is in the intergranular regions indicative of turbulent interactions between granules. There is also evidence of intermittent sources at all acoustic frequencies.

Energy from acoustic p-modes is converted to MHD modes and propagates along magnetic field lines in the pores. Observational evidence indicates the importance of high resolution studies for revealing the behaviour of acoustic energy flux in the solar atmosphere. [**?**] use high resolution data from the IMaX/Sunrise telescope to demonstrate that acoustic flux power, with periods greater than

100s carry at least half of the flux required to balance observed radiative losses in the solar Chromosphere. The main contrivution to theis flux is in the intergranular regions indicative of turbulent interactions between granules. There is also evidence of intermittent sources at all acoustic frequencies.

Studies of high resolution data from ground based observations and SDO AIA data by [**?**] investigates wave propagation in small scale structures such as pores. The

study indicated mechanisms for the propagation of energy from the Chromosphere to the Corona. For example running penumbral waves are frequently observed in sunspots these waves expand radially from the inner to the outer edges of the penumbra, they have a significant vertical component. Upwardly propagating waves were observed to propagate with a vertical velocity of $42 \pm 21 km/s$ and an delivering energies of approximately $150 W/m^2$, this is a small contribution to the required amount. The penumbral waves in sunspots possess a significant vertical component, this is presented as strong evidence of p-modes in the solar atmosphere propagating to the Corona.

There is a large body of computational work already undertaken Among others the following [**?**] et al study the Oscillatory Response of the 3D Solar Atmosphere to the Leakage of Photospheric Motion results are discussed in detail: i) High-frequency waves are shown to propagate from the lower atmosphere across the transition region, experiencing relatively low reflection, and transmitting most of their energy into the corona; ii) the thin transition region becomes a wave guide for horizontally propagating surface waves for a wide range of driver periods, and particularly at those periods that support chromospheric standing waves; iii) the magnetic field acts as a waveguide for both high- and low-frequency waves originating from the photosphere and propagating through the transition region into the solar corona.

Previous work has considered either point source drivers with a gaussian velocity distribution Other work e.g. by K. Murawski, T.V. Zaqarashvili (2010) [13] has demontrated that The numerical simulations show that the strong initial pulse may lead to the quasi periodic rising of chromospheric material into the lower corona in the form of spicules Khomenko and SantaMaria [**?**]. Kalkofen [14] considered the propagation of acoustic modes in a stratified hydrodynamical model of the solar atmosphere, they employed a cylindrically symmetric driver with a diameter of approximately $1 Mm$. They conclude that for driving regions of sizes smaller than the atmospheric scale height they are able to reproduce expansion waves which are characteristic of Chromospheric bright points. With a weak horizontal magnetic field, the physics within the interior of supergranulation cells [15] is suitably simple for undertaking hydrodynamic modelling. The objective of the work presented here is to characterise the dynamics generated by these solar global oscillating eigenmodes generated in the solar atmosphere. These modes ARE some sort of global eigenmodes. The coherence length of eigenoscillations at the photoshphere is about a few Mm, and the power peaks at around 3-5 mins.

It is understood that magnetic field lines suppress the p-mode oscillations [16] Sensitivity of p-mode absorption on magnetic region properties and kernel functions This has been corroborated further by the work of [17] demonstrating that the Interaction of p modes with a collection of thin magnetic tubes (article) recently konkol et al (2012) [18] have demonstrated that velocity pulses result in oscillatory phenomena with a periods of a few minutes. There two dimensional simulations demnstrate that the periods of the oscillations are dependent on the amplitude and vertical location of the initial pulse. There model considers such propagation in a magnetised atmosphere with a non vertical field. Hindman [19], considered driven acoustic Oscillations within a vertical magnetic field was considered. The study was extended by [20] who demonstrated that the inclined magnetic field lines provide the favourable conditions for leakage of p-modes into solar atmosphere and generation of spicules. Marsh [21] provided evidence of signal propagation from the transition region to corona 3 min period band, such propagation occured along fieldlines this is also reported by [22]. A recurring theme in many re-

sults is the observation that 3 min oscillations at transition region are related to 5 min global p-modes. There are two main view points for considering the mode conversion behaviour. These are to consider the chromosphere as resonant cavity and the behaviour of thecut off frequency. Considering the magnetohydrodynamic modes a detailed review was prepared by [23].

We consider the behaviour of these modes in a non magnetic atmosphere, an atmosphere with a uniform magnetic field and with magnetic flux tubes of different widths.

3. Numerical Computation Methods

To model the time-dependent evolution of photospheric oscillations in the solar atmosphere we solve the 3D ideal MHD equations. The 3D numerical simulations described here here were undertaken using SMAUG, the GPU implementation of the Sheffield Advanced Code (SAC)[24][25]. SAC and SMAUG are numerical MHD solvers allowing the simulation of a variety of physical processes in magnetised plasmas. With the upper boundary of our model in the Solar Corona and the lower boundary in the photosphere the SMAUG code is well suited for modelling the leakage of wave energy from the photopshere, through the transition zone and into the photosphere. With open boundary conditions for the lower and upper boundaries it is possible to model wave propagation for time scales characterised by the 5 minute p-mode induced oscillations. The general system of MHD equations are

$$\frac{\partial \rho}{\partial t} + \nabla \cdot (\mathbf{v}\rho) = 0, \tag{1}$$

$$\frac{\partial (\rho \mathbf{v})}{\partial t} + \nabla \cdot (\mathbf{v}\rho\mathbf{v} - \mathbf{B}\mathbf{B}) + \nabla p_t = \rho \mathbf{g}, \tag{2}$$

$$\frac{\partial e}{\partial t} + \nabla . (\mathbf{v}e - \mathbf{B}\mathbf{B} \cdot \mathbf{v} + \mathbf{v}p_t) + \nabla p_t = \rho \mathbf{g} \cdot \mathbf{v}, \tag{3}$$

$$\frac{\partial \mathbf{B}}{\partial t} + \nabla \cdot (\mathbf{v}\mathbf{B} - \mathbf{B}\mathbf{v}) = 0. \tag{4}$$

In these equations ρ is the mass density, $\mathbf{v}$ is the velocity, $\mathbf{B}$ is the magnetic field, e is the energy density, p_t is the total pressure and $\mathbf{g}$ is the gravitatioanl acceleration vector.

The total pressure p_t is written as

$$p_t = p_k + \frac{\mathbf{B}^2}{2}, \tag{5}$$

where p_k is the kinetic pressure given by

$$p_k = (\gamma - 1)(e - \frac{\rho \mathbf{v}^2}{2} - \frac{\mathbf{B}^2}{2}). \tag{6}$$

The equations (1) to (6) are applicable to an ideal compressible plasma. The SAC code is based on perturbed versions of these equations, thus the variables ρ, e and $\mathbf{B}$ are expressed in terms of perturbed and background quantities as

$$\rho = \tilde{\rho} + \rho_b, \tag{7}$$

$$e = \tilde{e} + e_b, \tag{8}$$

$$\mathbf{B} = \tilde{\mathbf{B}} + \mathbf{B}_b. \tag{9}$$

where $\tilde{\rho}$ is the perturbed density, $\tilde{e}$ is the perturbed energy and $\tilde{\mathbf{B}}$ is the perturbed magnetic field. The background quantities with a subscript b do not change in time, as we assume a magneto-hydrostatic equilibrium of the background plasma which may have a gravitational field present, denoted by $\mathbf{g}$. Hyper-diffusion and hyper-resistivity [26] are implemented to achieve numerical stability of the computed solution of the MHD equations. The full set of MHD equations, including the hyper-diffusion source terms are given in [24][25].

4. Solar Atmospheric Model

In order oscillatory phenomena in the Solar Corona a physically representative model of the solar atmosphere is needed. An option is the use of a parametrisation of the tempearture of the solar atmosphere which may be a smoothed step function profile [13]. Results have demonstrated the need for observationally derived semi-emprical models of the solar atmosphere. There is much discussion about model validity and the work undertaken to demonstrate the reliability of the assumptions used to construct realistic models of the solar chromosphere [27], [28]. The contention arises from the dynamical nature of the solar chromosphere for example local dynamo action has been suggested as a mechanism of Joule heating in the solar chromosphere [29]. The model atmosphere employed here is an observationally derived semi-empirical representation of the quiet sun. With the fundamental assumption of hydrostatic equilibrium a model of the chromosphere in equilibrium is constructed using the VALIIc model [4]. For the region of the solar atmosphere above 2.5Mm the results of the energy balance model of solar coronal heating has been used [30], this model includes an acoustic contribution comparable to the hydrostatic pressure.

5. Numerical Drivers for p-Mode Oscillations

The overview of observational studies identified a range of physical phenomena resulting in oscillatory behaviour and delivering energy into the solar atmosphere. The results presented here extend earlier work undertaken by [31], for their study point drivers were used to represent periodic buffeting or turbulent motions in the photosphere. The point driver is described by (10) has width Δx of $4Mm$ and width Δz of $4km$ applied to a 2D model of the realistic solar atmosphere. The results of the study demosnstrated surface wave phenomena and structures in the transition zone and highlighted the characteristics of the oscillatory phenomena as a result of frequency cutoffs induced by the stratified solar atmosphere.

$$V_z = A \sin\left(\frac{2\pi t}{T_s}\right) \exp\left(\frac{-(x-x_0)^2}{\Delta x^2}\right) \exp\left(\frac{-(z-z_0)^2}{\Delta z^2}\right), \tag{10}$$

For this study the model requires a driver mimicing the solar global oscillations. In the real Sun, photospheric p-mode oscillations have a horizontal wavelength and coherence. Here, these excitations are represented with a vertical velocity driver located at the

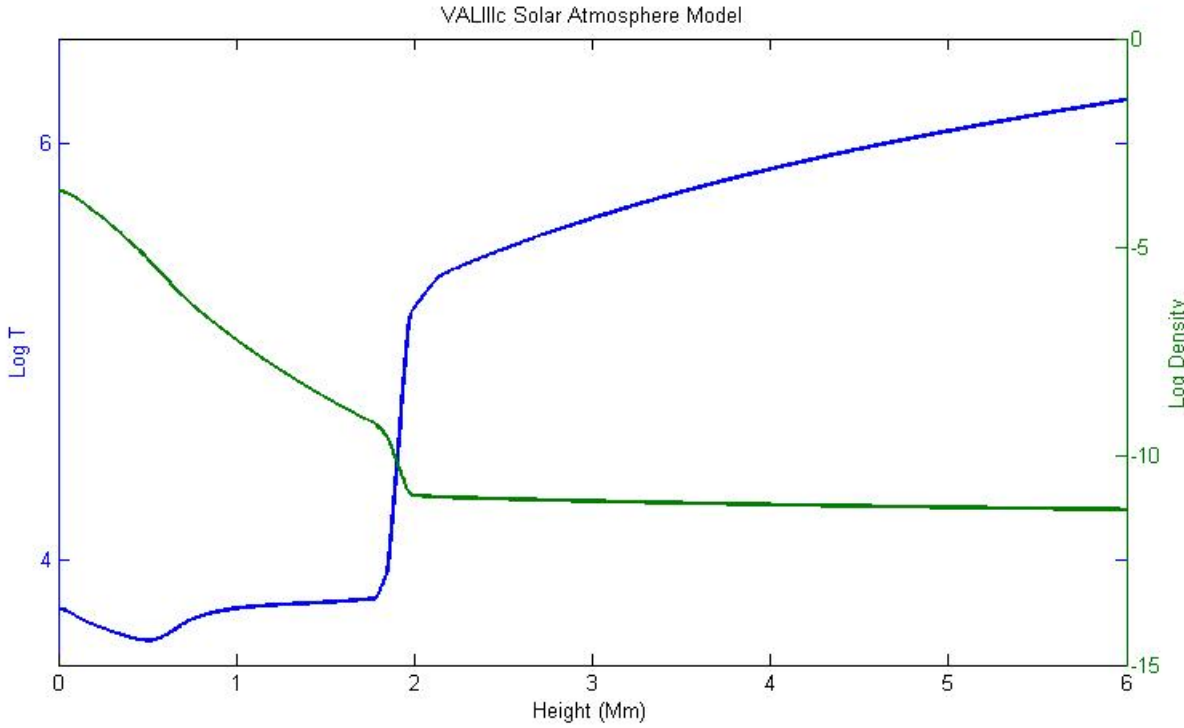

Figure 1: Temperature and Density Profiles Used for the Model Atmosphere.

photosphere, this acoustic p-mode driver excites waves which propagate into a realisitc 3D model of the Solar atmosphere. Drivers representing different modes are considered, for example an extended driver with a sinusoidal dependence and a wavelength of 8 Mm applied along the middle of the base of a computational domain of dimension 4Mm represents a fundamental mode. A driver with wavelength 4 Mm applied the same way represents the first harmonic. a second harmonic with wavelength 2Mm was also considered. Drivers may be constructed as an ensemble of these solar global eigenmodes. The vertical location of this extended driver is the temperature minimum which is $0.5Mm$ above the lower boundary of the model i.e. the photosphere. Such a driver may be represented by an equation such as (11)

$$V_z = A_{nm} \sin\left(\frac{2\pi t}{T_s}\right) \sin\left(\frac{(n+1)\pi x}{L_x}\right) \sin\left(\frac{(m+1)\pi y}{L_y}\right) \exp\left(\frac{-(z-z_0)^2}{\Delta z^2}\right), \qquad (11)$$

Here, we undertake simulations for different modes of oscillation where the mode is defined by the index n and m in equation (11) and (10). Since we are investigating the leakage of energy into the solar atmosphere, for consistency it is necessary to ensure that for the different modes the driver amplitude is set to a value which provides the same total amount of energy over the model cross section and per unit time. For the n, m

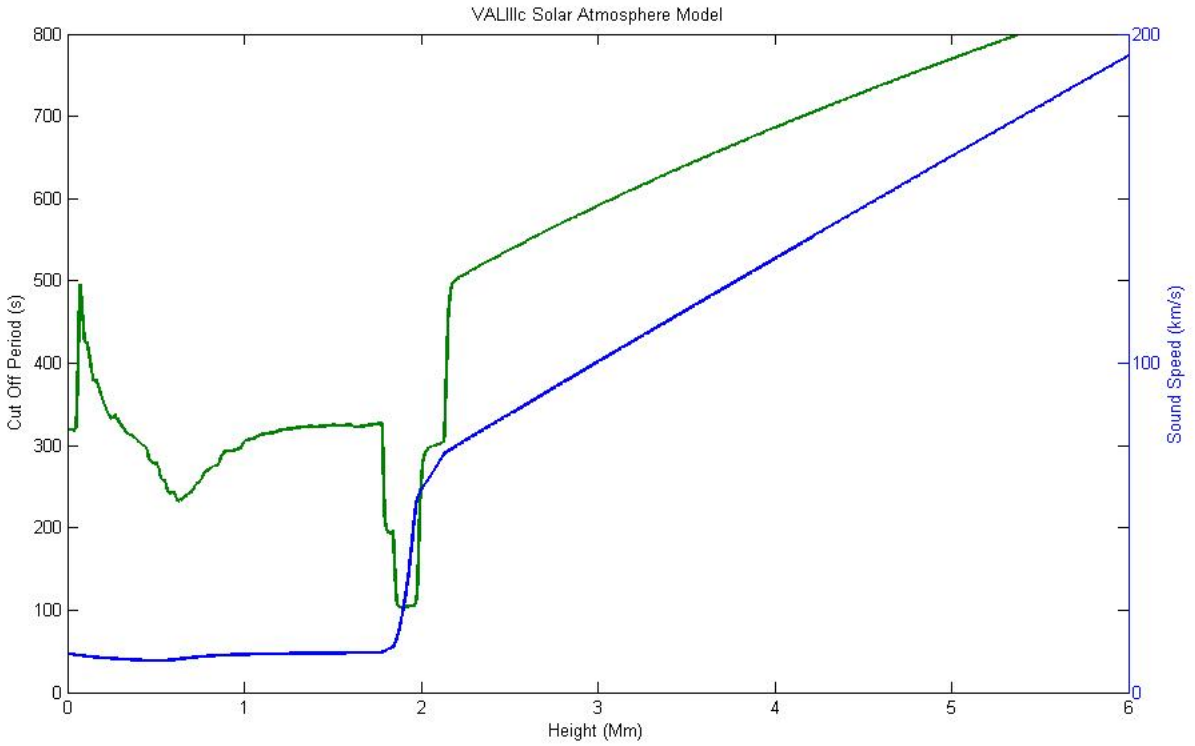

Figure 2: Sound Speed Profile for the Model Atmosphere.

mode the energy, E_{nm} may be written as;

$$E_{nm}(z,t) = \rho A_{nm}^2 I_{nm} \sin\left(\frac{2\pi t}{T_s}\right)^2 \exp\left(\frac{-(z-z_0)^2}{\Delta z^2}\right)^2, \tag{12}$$

The integral over expression I_{nm} is,

$$I_{nm} = \int_{-L_x}^{L_x}\int_{L_y}^{+L_y} \sin\left(\frac{(n+1)\pi x}{L_x}\right)^2 \sin\left(\frac{(m+1)\pi y}{L_y}\right)^2, \tag{13}$$

It is necessary to determine the amplitude A_{mn} for the different modes (n,m) with driver period T_s. This is achieved by computing the membrane energy integrated over the surface area and over a period of time from $t = 0$ to $t = T_m$ where T_m will correspond to the period of the driver with the largest value for the period. Using [1] , for the fundamental mode with driver period $300s$, we set $A_{00} = 350ms^{-1}$. Using the expression (12) to derive the ratio of the membrane energy for the mode (n, m) with driver period T_s, the mode (0,0) with driver period T_{00} and

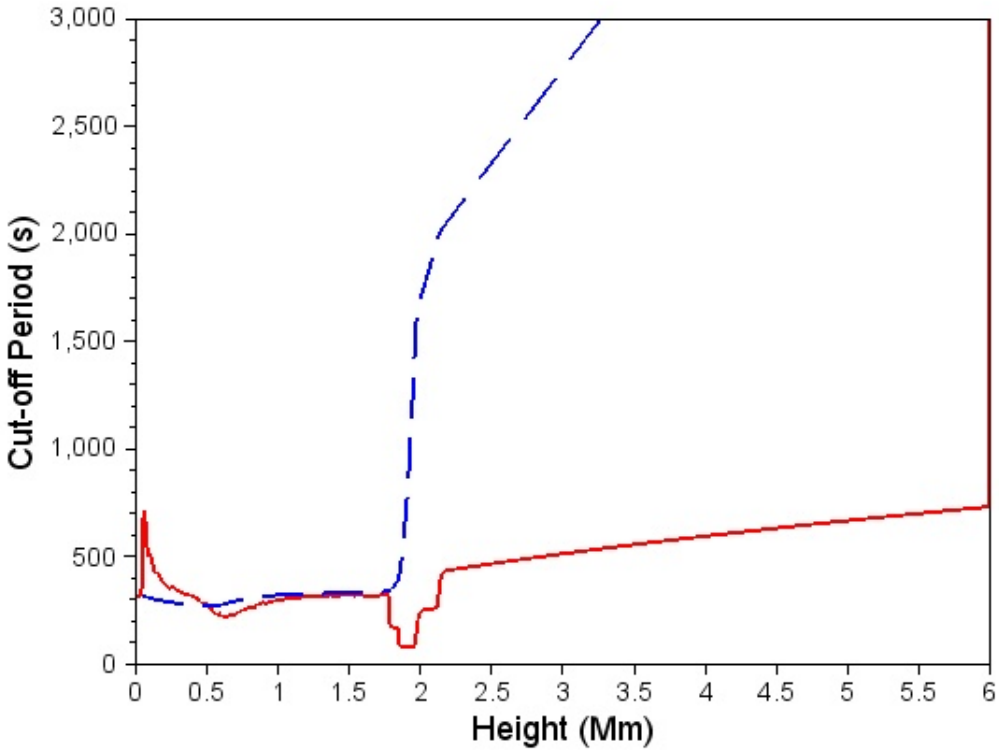

Figure 3: Cut of Frequency at Different Heights in the Model Solar Atmosphere.

making $L_x = L_y$ gives the relation

$$A_{nm}^2 = \frac{2A_{00}^2 T_{rat}}{(n^2 + m^2 + 2(n+m) + 2)} \tag{14}$$

where T_{rat} is

$$T_{rat} = \frac{T_m - \frac{T_{00}}{4\pi}\sin(\frac{4\pi T_m}{T_{00}})}{T_m - \frac{T_s}{4\pi}\sin(\frac{4\pi T_m}{T_s})} \tag{15}$$

This relation was used to determine the amplitudes for the higher order modes, starting from the A_{00} mode we used $A_{00} = 500ms^{-1}$.

6. Hydrodynamic Simulations

Simulations have been undertaken for a selection of drivers covering a range of time periods, modes and amplitudes. For this investigation we have been guided by the requirement that different driver modes deliver the same total amount of energy over the

Set	Description
A	Modes for the 30s, 180s and 300s Driver.
B	Normal Modes corresponding to different values of c_s
C	Normal Modes for equal mode values (i.e. n=m)

Table 1: Sets of Simulations Used to Characterise Oscillatory Motions Arising from an Extended Photospheric Driver.

Mode	$c_s = 20km/s$	$c_s = 31.4km/s$
(0,0)	282.8	180.0
(0,1)	200.0	127.3
(0,2)	133.3	84.8
(0,3)	100.0	63.6

Table 2: Time Periods of Extended Photospheric Drivers for Normal Modes Corresponding to c_s at Different Heights.

model cross section and when integrated over a time interval corresponding to the period of the longest period driver used for the set of simulations. Three sets of simulations have been considered, set A are the drivers selected because of their period, Set B are series of normal modes and Set C are normal modes with equal mode numbers 6. The amplitudes for each of the modes has determined using equation (14), to use this relation we assume that the (0,0) for the 300s driver has an amplitude of 350m/s [1].

The driver periods for set A correspond to the dominant atmospheric modes of oscillation for example the 5 minute mode and the 3 minute chromospheric mode. The 30s driver was selected because this corresponds to a frequency below that of the atmospheric cutoff and we can use the propagation characteristics as a test of our simulations. The periods for the normal modes were determined for different values of the speed of sound (c_s) in the solar atmosphere at different heights. The periods for the resulting drivers are shown in table 6.

$$\omega_{nm}^2 = 2\left(\frac{\pi c}{L}\right)^2, \tag{16}$$

$$c_s = \frac{\omega}{k}, \tag{17}$$

With the objective of characterising and understanding the nature of the frequencyy shifts of the excited modesWe consider a number of cases.

Since we want to investigate how wave energy propagation is influenced by the wave modes and frequencies, we compute the time averaged wave energy flux integrated over

Mode	Period (s)
(1,1)	471.4
(2,2)	235.7
(3,3)	157.1

Table 3: Time Periods of Extended Photospheric Drivers for Normal Modes Corresponding to Equal Mode Numbers.

Mode	Amplitude for 30s	Amplitude for 180s	Amplitude for 300s
(0,0)	343.4	348.3	350.0
(0,1)	217.2	220.3	221.4
(0,2)	153.6	155.8	156.5
(0,3)	117.8	119.5	120.0

Table 4: Amplitudes of Extended Photospheric Drivers for Modes with Different Driver periods.

Label	Density Profile	Gravity Enabled	Driver
B	VALIIC	yes	single driver at photosphere
C	VALIIC	no	single driver at photosphere
D	constant density	yes	single driver at photosphere
E	constant density	no	single driver at photosphere
F	constant density	no	two drivers at the photosphere and transition zone.

Table 5: Simulations Used to Characterise Oscillatory Motions Arising from the Surface Driver.

the cros-sectional area of the simulation box at different heights. The area of integration is perpendicular to the model z axis.

$$F_{int} = \frac{1}{t_{max}} \int_0^{t_{max}} \int \mathbf{F_{wave}} \cdot \mathbf{dAdt}, \tag{18}$$

Where the wave energy flux $\mathbf{F_{wave}}$ is given by

$$\mathbf{F_{wave}} = \tilde{\mathbf{p}}_\mathbf{k}\mathbf{v} + \frac{\mathbf{1}}{\mu_\mathbf{0}}(\mathbf{B_b} \cdot \tilde{\mathbf{B}})\mathbf{v} - \frac{\mathbf{1}}{\mu_\mathbf{0}}(\mathbf{v} \cdot \tilde{\mathbf{B}})\mathbf{B_b} \tag{19}$$

We have used the expression for the wave energy fluxused by $\tilde{p}_k$ is the perturbed kinetic pressure given by [**?**]

$$\tilde{p}_k = (\gamma - 1)(\tilde{e} - \frac{(\tilde{\rho} + \rho_b)\mathbf{v}^2}{2} - \frac{\tilde{\mathbf{B}}^2}{2} - \mathbf{B_b} \cdot \tilde{\mathbf{B}}). \tag{20}$$

7. Observations and Discussion

The propagation of waves in a stratified atmosphere can be understood using linearised versions of the equation of continuity, momentum and energy. Such atmospheric waves of expansion have been considered for many years [32].

Owing to the high gradients, partial reflection of acoustic waves at all frequencies is expected at the transition region. The transition region is the upper boundary of the chromospheric cavity, it has been previously suggested that this is the source of three-minute transition-region oscillations [3].

	1Mm	2Mm	4Mm	5.5Mm
30	0.0133	$1.7275\text{x}10^{-4}$	$1.0561\text{x}10^{-4}$	$5.5399\text{x}10^{-5}$
300	0.2607	0.008144	0.002176	0.001119
180	0.7227	0.047895	0.019831	0.010365
435.1	1.9415	0.043601	0.005944	0.003147
179.98	1.6450	0.004502	0.002600	0.001366
282.84	0.1986	0.004007	0.001845	$9.7821\text{x}10^{-4}$

Table 6: (00) mode energy ratio.

	1Mm	2Mm	4Mm	5.5Mm
30	0.0065	$1.751\text{x}10^{-5}$	$1.2579\text{x}10^{-6}$	$4.6820\text{x}10^{-7}$
300	0.1001	$8.796\text{x}10^{-4}$	$4.1494\text{x}10^{-6}$	$1.3059\text{x}10^{-6}$
180	0.1543	$5.8381\text{x}10^{-4}$	$3.2715\text{x}10^{-5}$	$1.1343\ \text{x}10^{-5}$
307.1	0.0982	0.001	$4.1351\text{x}10^{-6}$	$1.3380\ \text{x}10^{-6}$
127.27	0.0829	$4.3190\text{x}10^{-4}$	$5.1387\text{x}10^{-5}$	$2.0397\ \text{x}10^{-5}$
200.0	0.1126	$4.4180\text{x}10^{-4}$	$2.0186\text{x}10^{-5}$	$6.3062\ \text{x}10^{-6}$

Table 7: (01) mode energy ratio.

	1Mm	2Mm	4Mm	5.5Mm
30	0.0024	$7.2158\ \text{x}10^{-6}$	$1.0651\text{x}10^{-6}$	$7.6079\text{x}10^{-7}$
300	0.0578	$4.9604\ \text{x}10^{-4}$	$5.5618\text{x}10^{-6}$	$4.1907\text{x}10^{-6}$
180	0.0687	$3.5547\ \text{x}10^{-4}$	$6.0675\text{x}10^{-5}$	$4.1492\ \text{x}10^{-5}$
205.1	0.3135	0.0015	$1.6520\text{x}10^{-4}$	$1.1272\text{x}10^{-4}$
84.84	0.0206	$5.8903\ \text{x}10^{-5}1.6520\ \text{x}10^{-5}$	$1.1890\ \text{x}10^{-5}$	
133.33	0.0497	$1.9731\text{x}10^{-4}7.9834\ \text{x}10^{-5}$	$5.6267\ \text{x}10^{-5}$	

Table 8: (02) mode energy ratio.

	1Mm	2Mm	4Mm	5.5Mm
30	0.0101	$4.2736\text{x}10^{-5}$	$6.3291\text{x}10^{-7}$	$3.7786\text{x}10^{-7}$
300	0.0359	$3.8929\text{x}10^{-4}$	$3.2621\text{x}10^{-7}$	$2.1259\text{x}10^{-7}$
180	0.0351	$1.3948\text{x}10^{-4}$	$3.1342\text{x}10^{-6}$	$1.8205\text{x}10^{-6}$
153.8	0.0313	$1.1043\text{x}10^{-4}$	$3.8071\text{x}10^{-6}$	$2.1034\text{x}10^{-6}$
63.63	0.0051	$9.8989\text{x}10^{-6}$	$7.0207\text{x}10^{-7}$	$4.0621\text{x}10^{-7}$
100.0	0.0151	$3.0678\text{x}10^{-5}$	$2.8527\text{x}10^{-6}$	$1.6707\text{x}10^{-6}$

Table 9: (03) mode energy ratio .

	1Mm	2Mm	4Mm	5.5Mm
(0,0)	0.7227	0.0479	0.0198	0.0104
(0,1)	0.1543	0.0006	$3.2715\text{x}10^{-5}$	$1.1343\text{x}10^{-5}$
(0,2)	0.0687	0.0004	$6.0675\text{x}10^{-5}$	$4.1492\text{x}10^{-5}$
(0,3)	0.0351	0.0001	$3.1342\text{x}10^{-6}$	$1.8205\ \text{x}10^{-6}$
(1,1)	0.4072	0.0011	$4.5311\text{x}10^{-6}$	$5.5495\text{x}10^{-7}$
(1,2)	0.3331	0.0012	$3.0728\text{x}10^{-6}$	$1.3055\text{x}10^{-6}$
(1,3)	0.2961	0.0011	$4.8733\text{x}10^{-7}$	$3.4760\text{x}10^{-7}$
(2,2)	0.3054	0.0011	$1.5844\text{x}10^{-5}$	$1.7622\text{x}10^{-5}$
(2,3)	0.2732	0.0008	$2.1443\text{x}10^{-6}$	$1.7045\text{x}10^{-6}$
(3,3)	0.2205	0.0006	$1.9711\text{x}10^{-7}$	$2.6756\text{x}10^{-7}$

Table 10: 180s driver energy ratio.

	1Mm	2Mm	4Mm	5.5Mm
(0,0)	0.2607	0.0081	$2.2\text{x}10^{-3}$	$1.1\text{x}10^{-3}$
(0,1)	0.1001	0.0009	$4.1494\text{x}10^{-6}$	$1.3059\text{x}10^{-6}$
(0,2)	0.0578	0.0005	$5.5618\text{x}10^{-6}$	$4.1907\text{x}10^{-6}$
(0,3)	0.0359	0.0004	$3.2621\text{x}10^{-7}$	$2.1259\text{x}10^{-7}$
(1,1)	0.2267	0.0016	$9.9329\text{x}10^{-7}$	$1.0749\text{x}10^{-7}$
(1,2)	0.2535	0.0016	$8.2058\text{x}10^{-7}$	$2.8814\text{x}10^{-7}$
(1,3)	0.2692	0.0023	$2.1995\text{x}10^{-7}$	$9.0161\text{x}10^{-8}$
(2,2)	0.2625	0.0021	$1.4846\text{x}10^{-6}$	$1.7399\text{x}10^{-6}$
(2,3)	0.2328	0.0017	$2.4839\text{x}10^{-7}$	$2.0699\text{x}10^{-7}$
(3,3)	0.2036	0.0012	$7.2069\text{x}10^{-8}$	$4.944\text{x}10^{-8}$

Table 11: 300s driver energy ratio percentage.

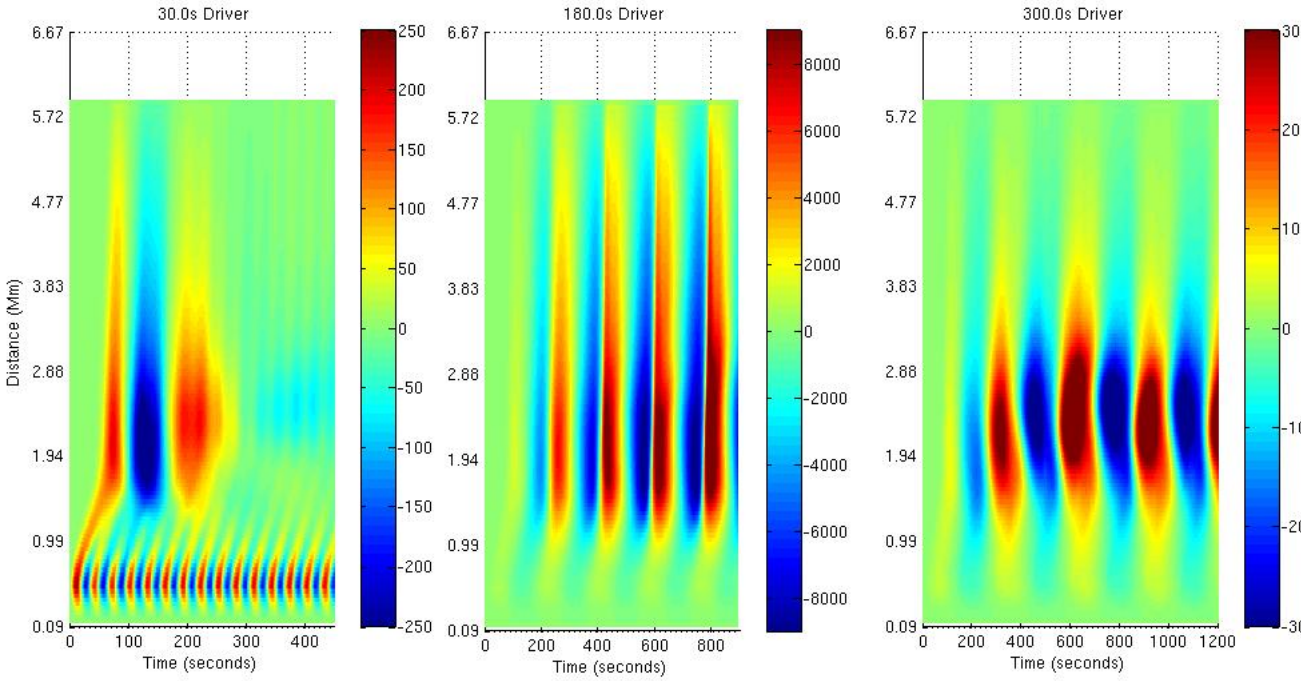

Figure 4: Distance time plot for fundamental model and 30s,180s and 300s driver period for the z component of the velocity for a vertical slice across the box taken at 2Mm and shows the profile of v_z through the solar atmosphere for different time steps.

It is known that the propagation of acoustic waves in an unbounded medium is determined by a cut-off period. In a gravitationally stratified atmosphere acoustic waves can only propagate if the wave period is less than the cut off. It was shown that this frequency is a resonance, disturnaces with this frequency trigger a response. Waves with a period greater than the cut-off are evanescent.

The propagation of these acoustic wave modes in a gravitationally stratified atmosphere is determined by characterised cut off frequencies, theory predicts that waves will only propagate if the wave period is less than the local acoustic cut-off period in the atmosphere.

Following [33] and solving the Klein-Gordon equation for the gravitationally stratified atmosphere (21) the cutoff for the atmosphere can be obtained (22)

$$\frac{\partial^2 Q}{\partial t^2} - c_s^2(z)\frac{\partial^2 Q}{\partial z^2} + \Omega^2(z)Q = 0, \tag{21}$$

$$P_c(z) = \frac{2\Lambda_0}{c_s(z)}\sqrt{\frac{1}{1+2\frac{d\Lambda_0(z)}{dz}}}, \tag{22}$$

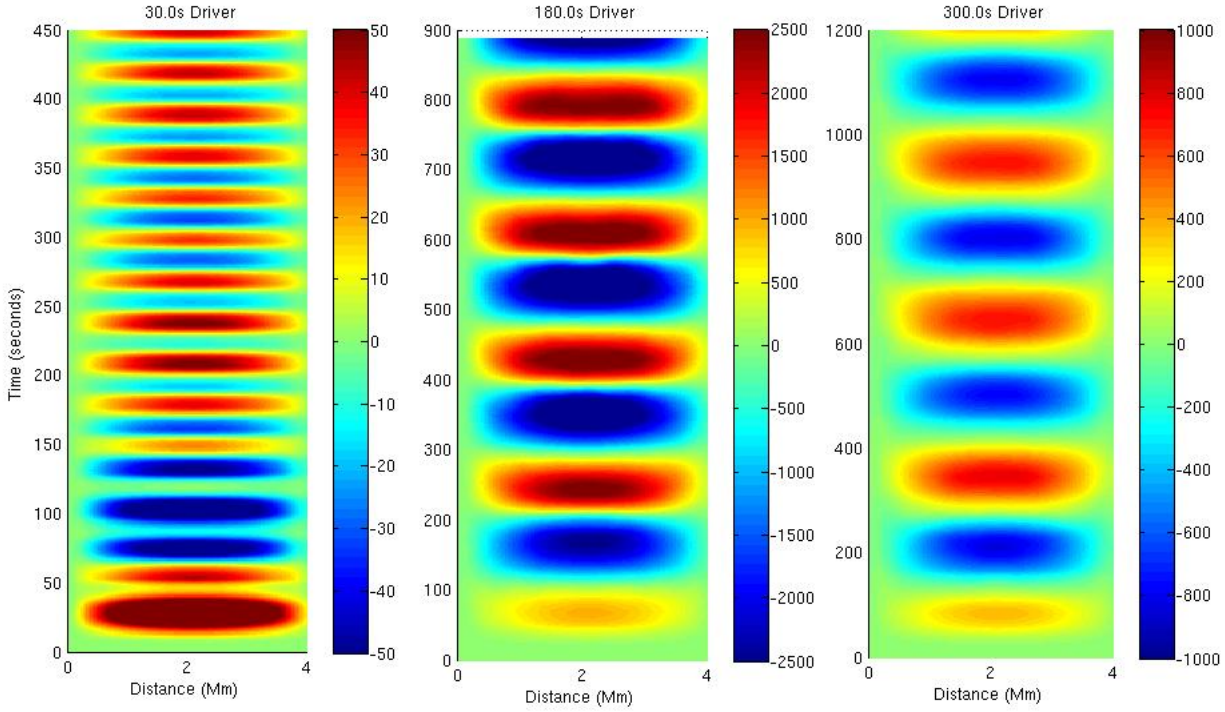

Figure 5: Distance time plot for fundamental model and 30s,180s and 300s driver period for the z component of the velocity for a horizontal slice across the box taken at 0.94Mm shows the profile of v_z across the simulation box at a given point in the solar chromosphere for different time steps.

The pressure scale height for an atmosphere stratified by a uniform gravitational field

$$\Lambda_0(z) = \frac{p_0(z)}{g\rho_0(z)}, \tag{23}$$

The variation of the cutoff with solar atmospheric height is shown in figure which shows the cutoff period for the VALIIIc atmopshere and for an isothermal atmosphere. Using this is an indicator of the propagation behaviour of the acoustic oscillations it is recognised from figure that there is a number of distinct regions of propagation behaviour. For the photosphere near the temperature minimum the cutoff period is 300s here it is expected that the 5 minutes modes are evanescent. In the chromosphere increases to a value greater than 300s, here the five minute modes can propagate. For the transition zone the cutoff drops to a value which goes down to 100s. In the corona it is seen that a much greater range of frequencies can propagate.

For the fundamental modes illustrated in figure 4, 5 and 6 we observe that there is no significant structure at the transition zone. However, the 30s mode is particulalry interesting detailed movies demonstrate the rapid expansion of the plume as it crosses the transition zone this is accompanied with an increase in the transverse velocity this observationi is true for both 180s, 30s and 300s driver scenarios. As the mode order is

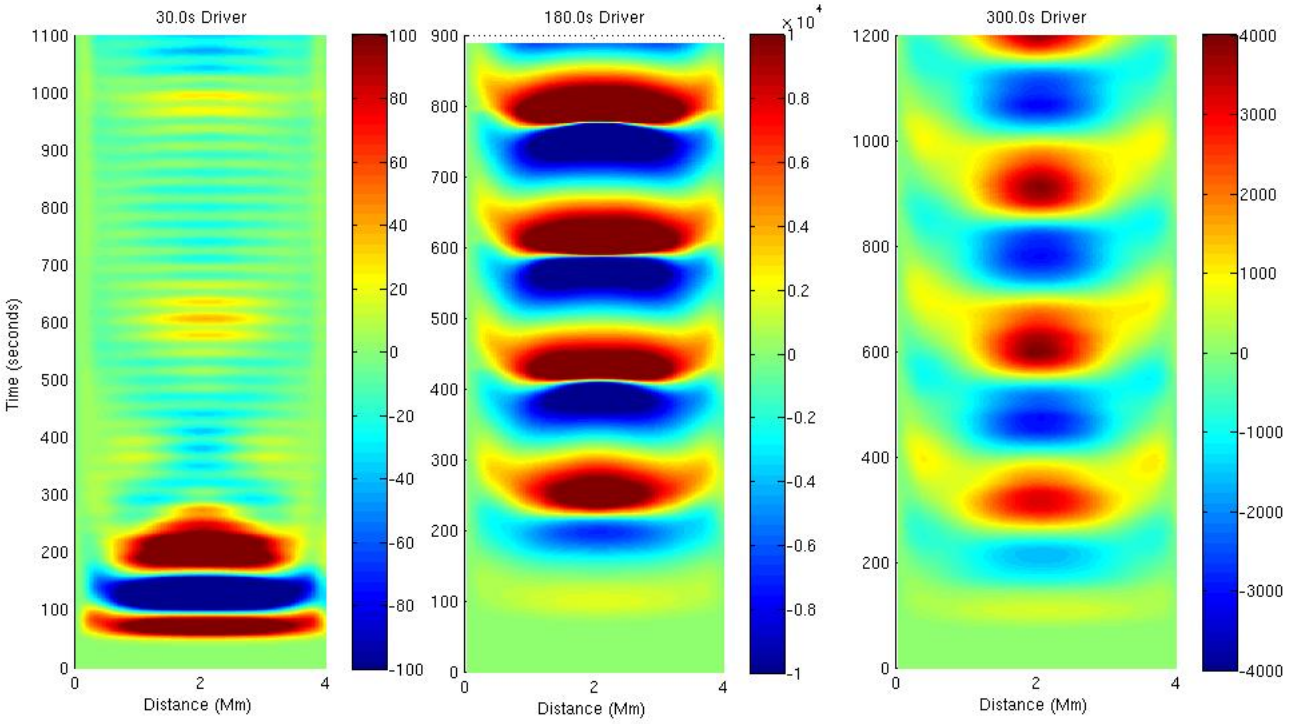

Figure 6: Distance time plot for fundamental model and 30s,180s and 300s driver period for the z component of the velocity for a horizontal slice across the box taken at the transition zone shows the profile of v_z across the simulation box at a height of 2Mm in the solar atmosphere for different time steps.

increased from $n = 0$, to $n = 1$ and then $n = 2$ its is observed that transition region structuring becomes apparent and is more reminiscent of the observations of [**?**].

For the fundamental modes with the 30s, 180s and 300s driver we have plotted distance-time diagrams of the z-component of the plasma velocity i.e. in the same direction as the driver and in the direction of increasing height through the solar atmosphere. Figure shows the distance time plots for a vertical section through the simulation box, since this was a fundamental mode the section was taken through the middle of the simulation box. The plots show that the greatest amplitude arises in the transition region in particular for the 180s driver. Looking at the result for the 30s driver it is seen that the initial travelling response reaches a response at around 0.5Mm corresponding to a cut-off of 200s. The maximum amplitude is coherent with the maximum occuring at the same frequency as that of the driver. For the first 70 periods maxima appear in the transition zone. It appears that the transition zone is essentially a source of excitation with freuency lower than that of the driver, however, at longer time periods these motions occur with reduced amplitude but with the same period as the driver. For the180s and 300s drivers it is observed that the amplitude in the transition zone is larger than that for the 30s driver by a factor of upto 20. For the 30,180 and 300s case we observe the travelling

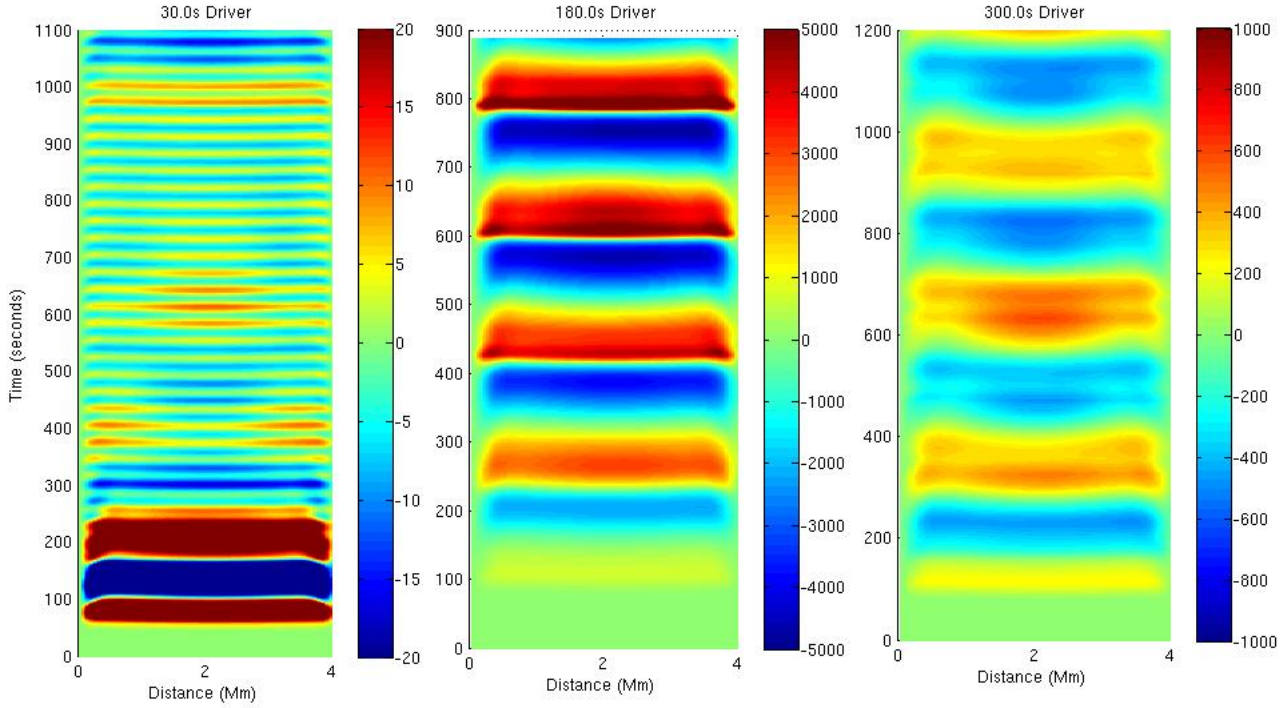

Figure 7: Distance time plot for fundamental model and 30s,180s and 300s driver period for the z component of the velocity for a horizontal slice across the box taken at 4.2Mm shows the profile of v_z across the simulation box at a given point in the solar atmosphere for different time steps.

wave in the Chromosphere and a stationary wave in the solar Corona. Although the 180s mode shows the greatest excitation both the 180s and 300s drivers become evanescent due the the cut-off for the upper atmosphere. Figure shows the distance time plot for a horizontal section taken at a height of 0.94Mm, i.e. through the Chromosphere. The travelling modes in these plots propagate as plane modes with a frequecy consistent with that of the driver. The greatest intensity is observed for the 180s driver. Propagation for the transition zone shown in figure shows the most powerful response for the 180s driver followed by the 300s driver. The response for the 30s driver decays rapidly after the first ten cycles. As we move into the Corona there is further attenuation with the greatest signal reduction for the 30s driver.

Figure shows three-dimensional snapshots of the evolution of V_z. This is for the fundamental mode driver with a period of 30s for the case of a nonmagnetic configuration.The figure shows profiles obtained at the times (a) t = 112 seconds, (b) t = 216 seconds, (c) t = 244 seconds, and (d) t = 316 seconds. The distance-time plot in figure shows a plot of the z-component of the velocity at different altitudes through the atmosperic configuration and at different time steps. The plot shows clearly the conversion of the 30s chromospheric mode to a slower mode propagating with a period of 180s [**?**].

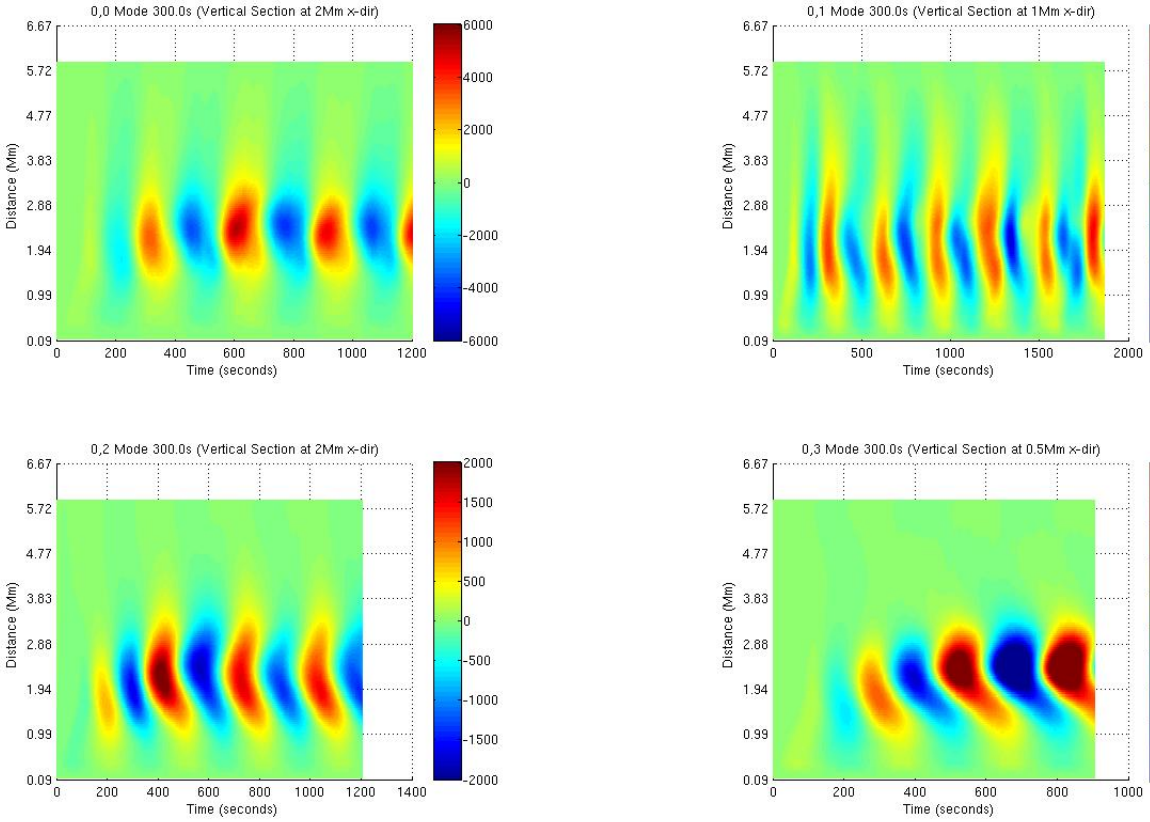

Figure 8: Distance time plot for fundamental model with 300s period for the z component of the velocity. x-direction

8. Conclusions

1. The results demonstrate the mode conversion of modes with a 30s period to modes with a 180s period [**?**]. This supports the idea that the chromosphere is a source for the 180s period oscillations.
2. Increased transition region structuring is observed for the higher order modes
3. Magnetic flux tube enhance the structruring in the transition zone

RE acknowledges M. Kéray for patient encouragement and is also grateful to NSF, Hungary (OTKA, Ref. No. K83133). The authors thank the Science and Technology Facilities Council (STFC), UK for the support they received. We acknowledge Corporate Information and Computing Services at The University of Sheffield for the provision of the High Performance Computing Service.

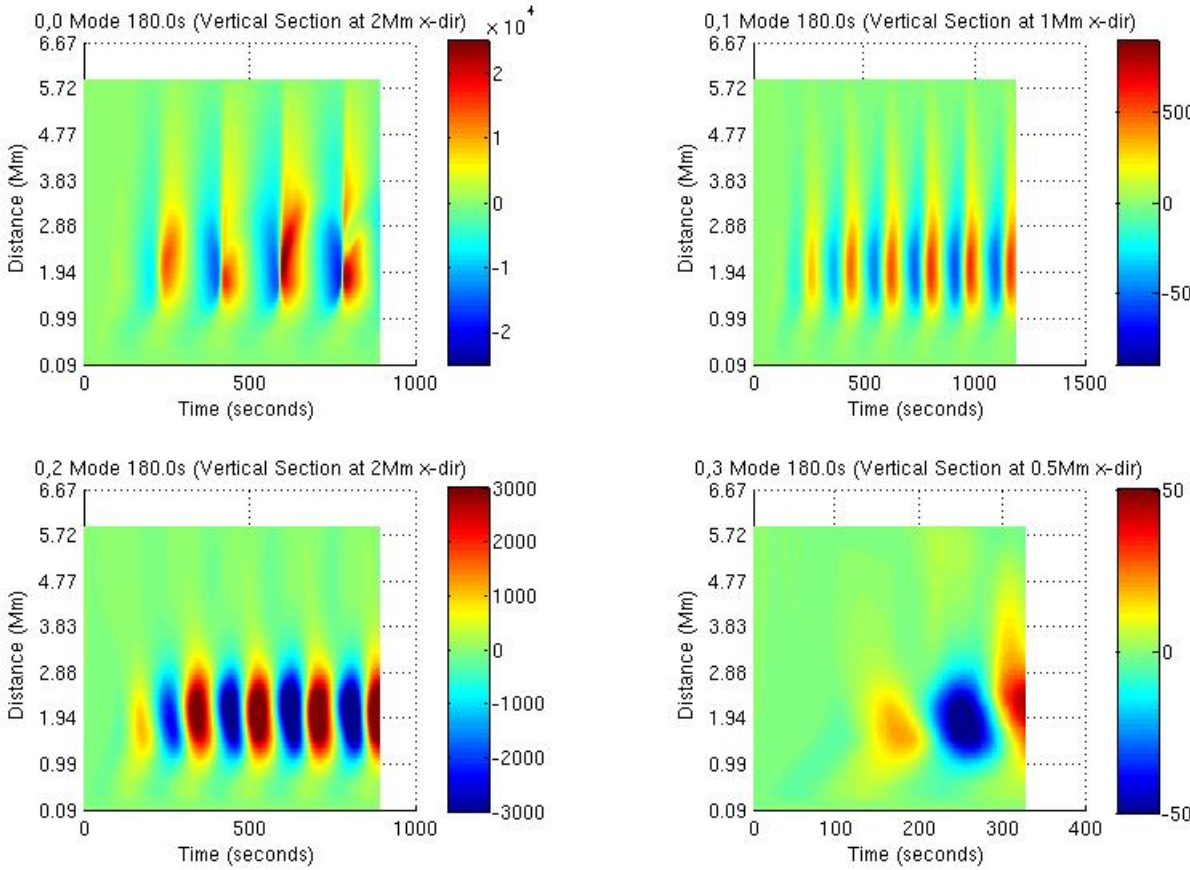

Figure 9: Distance time plot for fundamental model with 180s period for the z component of the velocity. x-direction

9. References

References

[1] R. B. Leighton, in: R. N. Thomas (Ed.), Aerodynamic Phenomena in Stellar Atmospheres, vol. 12 of *IAU Symposium*, 321–325, 1960.

[2] R. K. Ulrich, The Five-Minute Oscillations on the Solar Surface, ApJ 162 (1970) 993, doi:\let\ @tempa\bibinfo@X@doi10.1086/150731.

[3] J. W. Leibacher, R. F. Stein, A New Description of the Solar Five-Minute Oscillation, 7 (1971) 191–192.

[4] J. E. Vernazza, E. H. Avrett, R. Loeser, Structure of the solar chromosphere. III - Models of the EUV brightness components of the quiet-sun, 45 (1981) 635–725, doi:\let\@tempa\bibinfo@X@ doi10.1086/190731.

[5] B. Roberts, P. M. Edwin, A. O. Benz, On coronal oscillations, ApJ 279 (1984) 857–865, doi: \let\@tempa\bibinfo@X@doi10.1086/161956.

[6] I. De Moortel, An overview of coronal seismology, Philosophical Transactions of the Royal Society of London Series A 363 (2005) 2743–2760, doi:\let\@tempa\bibinfo@X@doi10.1098/rsta.2005.1665.

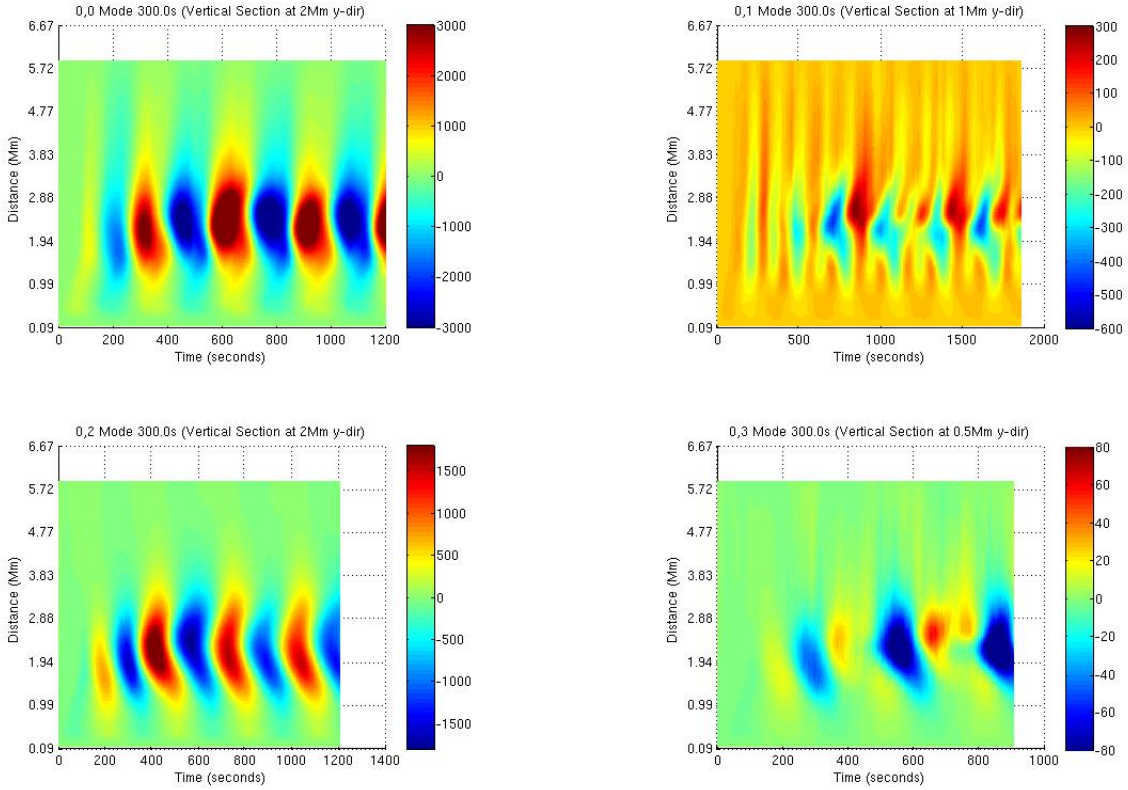

Figure 10: Distance time plot for fundamental model with 300s period for the z component of the velocity. y-direction

[7] C. Beck, R. Rezaei, K. G. Puschmann, The energy of waves in the photosphere and lower chromosphere. II. Intensity statistics, A&A 544 A46, doi:\let\@tempa\bibinfo@X@doi10.1051/0004-6361/201219242.

[8] M. Carlsson, R. F. Stein, Non-LTE radiating acoustic shocks and CA II K2V bright points, ApJL 397 (1992) L59–L62, doi:\let\@tempa\bibinfo@X@doi10.1086/186544.

[9] G. Cauzzi, K. P. Reardon, H. Uitenbroek, F. Cavallini, A. Falchi, R. Falciani, K. Janssen, T. Rimmele, A. Vecchio, F. Wöger, The solar chromosphere at high resolution with IBIS. I. New insights from the Ca II 854.2 nm line, A&A 480 (2008) 515–526, doi:\let\@tempa\bibinfo@X@doi10.1051/0004-6361:20078642.

[10] S. M. Jefferies, S. W. McIntosh, J. D. Armstrong, T. J. Bogdan, A. Cacciani, B. Fleck, Low-frequency magneto-acoustic waves in the solar chromosphere, in: Proceedings of SOHO 18/GONG 2006/HELAS I, Beyond the spherical Sun, vol. 624 of *ESA Special Publication*, 16.1, 2006.

[11] M. J. Penn, B. J. Labonte, The source of 5 minute period photospheric umbral oscillations, ApJ 415 (1993) 383–396, doi:\let\@tempa\bibinfo@X@doi10.1086/173172.

[12] T. J. Bogdan, Effect of Thermal Conduction on Acoustic Waves in Coronal Loops, ApJ 643 (2006) 532–539, doi:\let\@tempa\bibinfo@X@doi10.1086/502622.

[13] K. Murawski, T. V. Zaqarashvili, Numerical simulations of spicule formation in the solar atmosphere, A&A 519 A8, doi:\let\@tempa\bibinfo@X@doi10.1051/0004-6361/201014128.

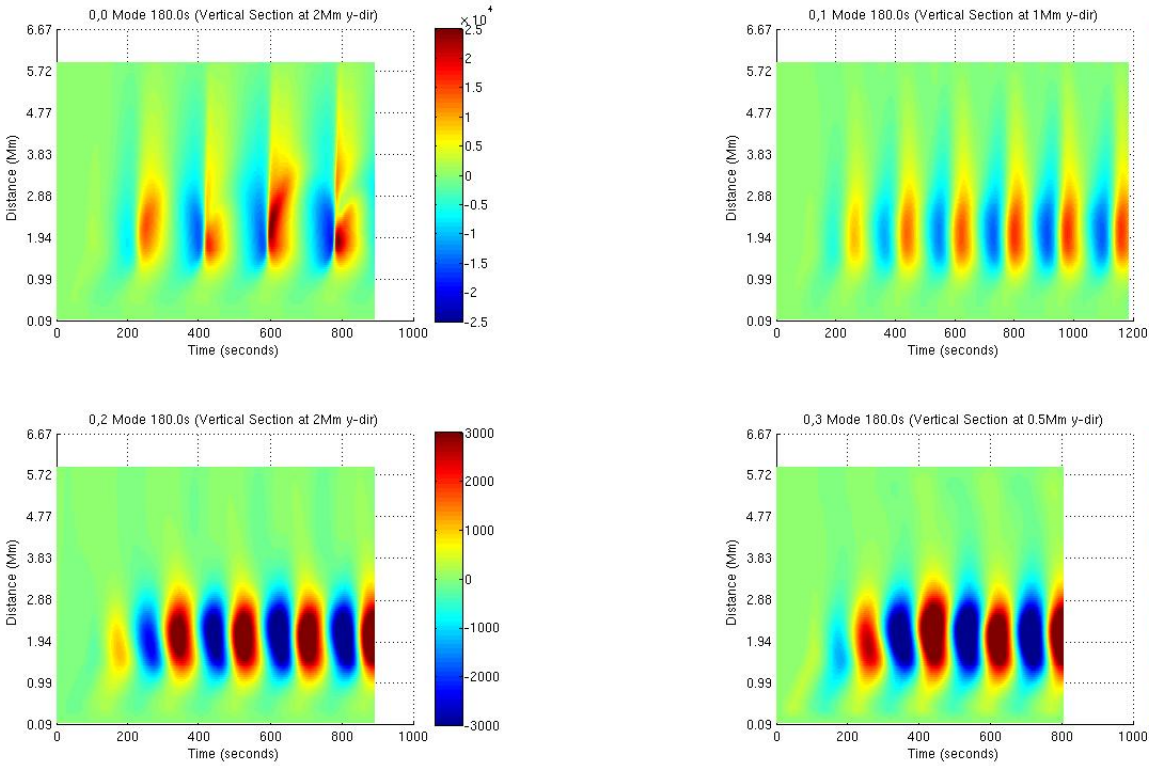

Figure 11: Distance time plot for fundamental model with 180s period for the z component of the velocity. y-direction

[14] W. Kalkofen, P. Rossi, G. Bodo, S. Massaglia, Acoustic waves in a stratified atmosphere. IV. Three-dimensional nonlinear hydrodynamics, A&A 520 A100, doi:\let\@tempa\bibinfo@X@doi10.1051/0004-6361/200912996.

[15] B. W. Lites, M. Kubo, H. Socas-Navarro, T. Berger, Z. Frank, R. Shine, T. Tarbell, A. Title, K. Ichimoto, Y. Katsukawa, S. Tsuneta, Y. Suematsu, T. Shimizu, S. Nagata, The Horizontal Magnetic Flux of the Quiet-Sun Internetwork as Observed with the Hinode Spectro-Polarimeter, ApJ 672 1237-1253, doi:\let\@tempa\bibinfo@X@doi10.1086/522922.

[16] A. Gascoyne, R. Jain, B. W. Hindman, Sensitivity of p-mode absorption on magnetic region properties and kernel functions, A&A 526 A93, doi:\let\@tempa\bibinfo@X@doi10.1051/0004-6361/201015898.

[17] R. Jain, A. Gascoyne, B. W. Hindman, Interaction of p modes with a collection of thin magnetic tubes, 415 (2011) 1276–1279, doi:\let\@tempa\bibinfo@X@doi10.1111/j.1365-2966.2011.18778.x.

[18] P. Konkol, K. Murawski, T. V. Zaqarashvili, Numerical simulations of magnetoacoustic oscillations in a gravitationally stratified solar corona, A&A 537 A96, doi:\let\@tempa\bibinfo@X@doi10.1051/0004-6361/201117943.

[19] B. W. Hindman, E. G. Zweibel, P. S. Cally, Driven Acoustic Oscillations within a Vertical Magnetic Field, ApJ 459 (1996) 760, doi:\let\@tempa\bibinfo@X@doi10.1086/176940.

[20] S. P. James, R. Erdélyi, B. De Pontieu, Can ion-neutral damping help to form spicules?, A&A 406 (2003) 715–724, doi:\let\@tempa\bibinfo@X@doi10.1051/0004-6361:20030685.

[21] M. S. Marsh, R. W. Walsh, p-Mode Propagation through the Transition Region into the Solar

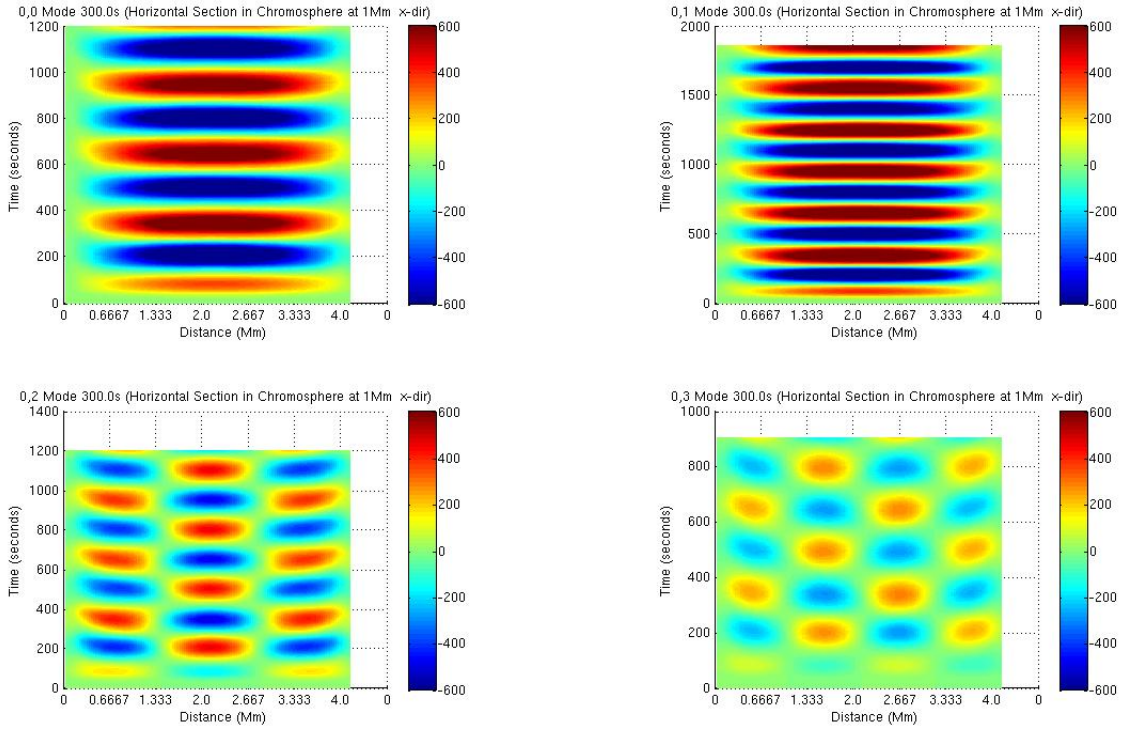

Figure 12: Distance time plot for modes with 300s period Horizontal Section through the Chromosphere (at 1Mm) for the z component of the velocity. x-direction

Corona. I. Observations, ApJ 643 (2006) 540–548, doi:\let\@tempa\bibinfo@X@doi10.1086/501450.

[22] V. I. Zhukov, Oscillations on the Sun in regions with a vertical magnetic field. I. Sunspot umbral oscillations, A&A 386 (2002) 653–657, doi:\let\@tempa\bibinfo@X@doi10.1051/0004-6361:20020279.

[23] E. Khomenko, I. Calvo Santamaria, Magnetohydrodynamic waves driven by p-modes, Journal of Physics Conference Series 440 (1) 012048, doi:\let\@tempa\bibinfo@X@doi10.1088/1742-6596/440/1/012048.

[24] M. K. Griffiths, V. Fedun, R. Erdélyi, A Fast MHD Code for Gravitationally Stratified Media using Graphical Processing Units: SMAUG, Journal of Astrophysics and Astronomy 36 (2015) 197–223, doi:\let\@tempa\bibinfo@X@doi10.1007/s12036-015-9328-y.

[25] S. Shelyag, V. Fedun, R. Erdélyi, Magnetohydrodynamic code for gravitationally-stratified media, A&A 486 (2008) 655–662, doi:\let\@tempa\bibinfo@X@doi10.1051/0004-6361:200809800.

[26] S. E. Caunt, M. J. Korpi, A 3D MHD model of astrophysical flows: Algorithms, tests and parallelisation, A&A 369 (2001) 706–728, doi:\let\@tempa\bibinfo@X@doi10.1051/0004-6361:20010157.

[27] M. Carlsson, R. F. Stein, Does a nonmagnetic solar chromosphere exist?, ApJL 440 (1995) L29–L32, doi:\let\@tempa\bibinfo@X@doi10.1086/187753.

[28] W. Kalkofen, The Validity of Dynamical Models of the Solar Atmosphere, Sol. Phys. 276 (2012) 75–95, doi:\let\@tempa\bibinfo@X@doi10.1007/s11207-011-9898-z.

[29] J. Leenaarts, M. Carlsson, V. Hansteen, B. V. Gudiksen, On the minimum temperature of the quiet solar chromosphere, A&A 530 A124, doi:\let\@tempa\bibinfo@X@doi10.1051/0004-6361/201016392.

[30] R. W. P. McWhirter, P. C. Thonemann, R. Wilson, The heating of the solar corona. II - A model

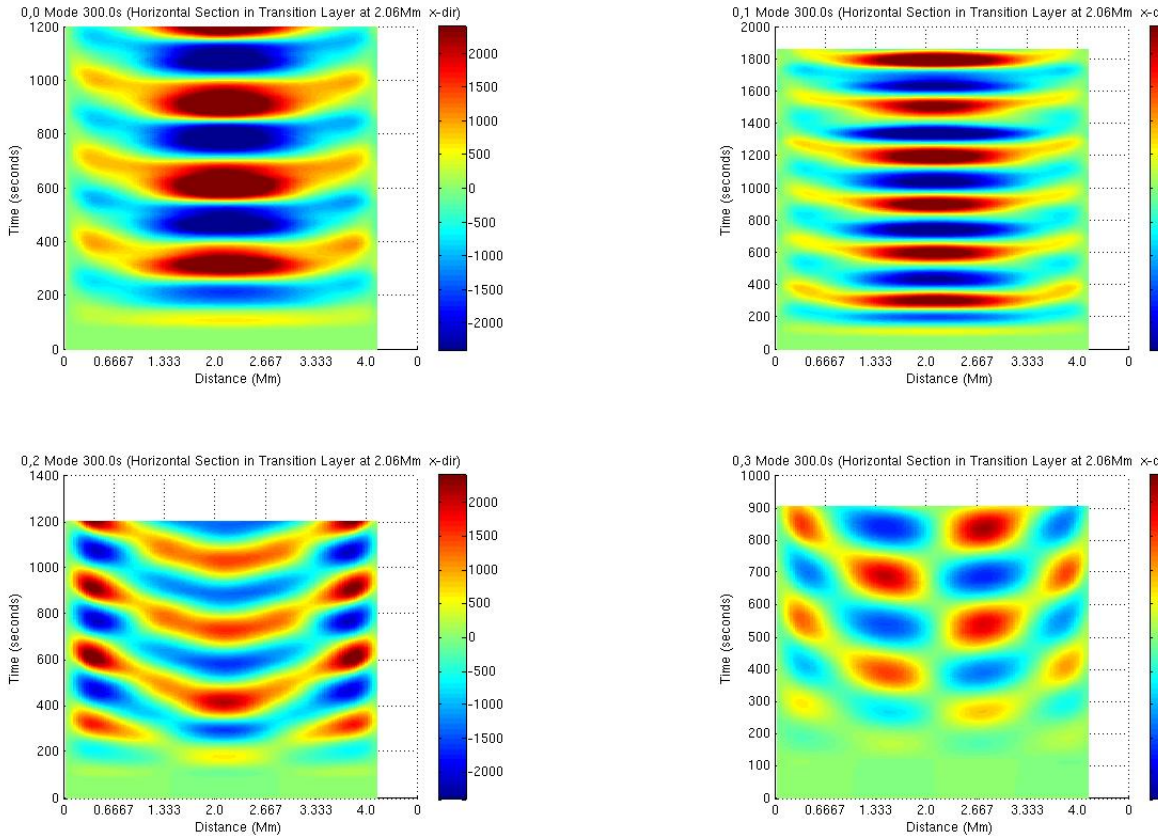

Figure 13: Distance time plot for modes with 300s period Horizontal Section through the Transition Region (at 2.06Mm) for the z component of the velocity. x-direction

based on energy balance, A&A 40 (1975) 63–73.

[31] C. Malins, On transition region convection cells in simulations of {p}-mode propagation, Astronomische Nachrichten 328 (2007) 752–755, doi:\let\@tempa\bibinfo@X@doi10.1002/asna.200710786.

[32] H. Lamb, Hydrodynamics, 1932.

[33] Y. Taroyan, R. Erdélyi, Global Acoustic Resonance in a Stratified Solar Atmosphere, Sol. Phys. 251 (2008) 523–531, doi:\let\@tempa\bibinfo@X@doi10.1007/s11207-008-9154-3.

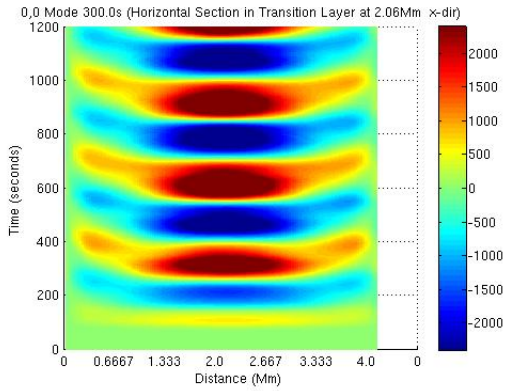

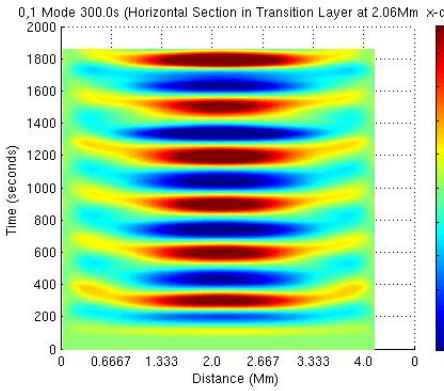

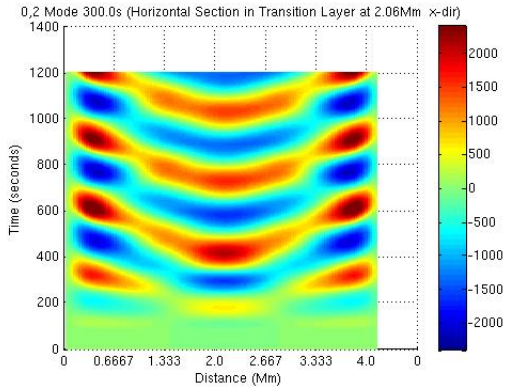

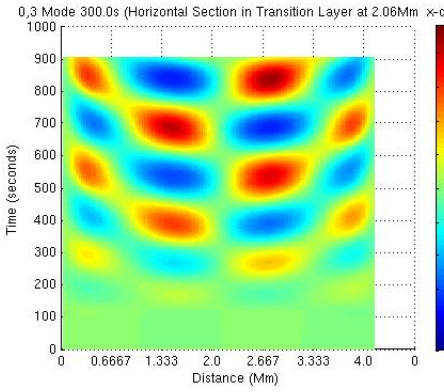

Figure 14: Distance time plot for modes with 300s period Horizontal Section through the Solar Corona (at 4.3Mm) for the z component of the velocity. x-direction

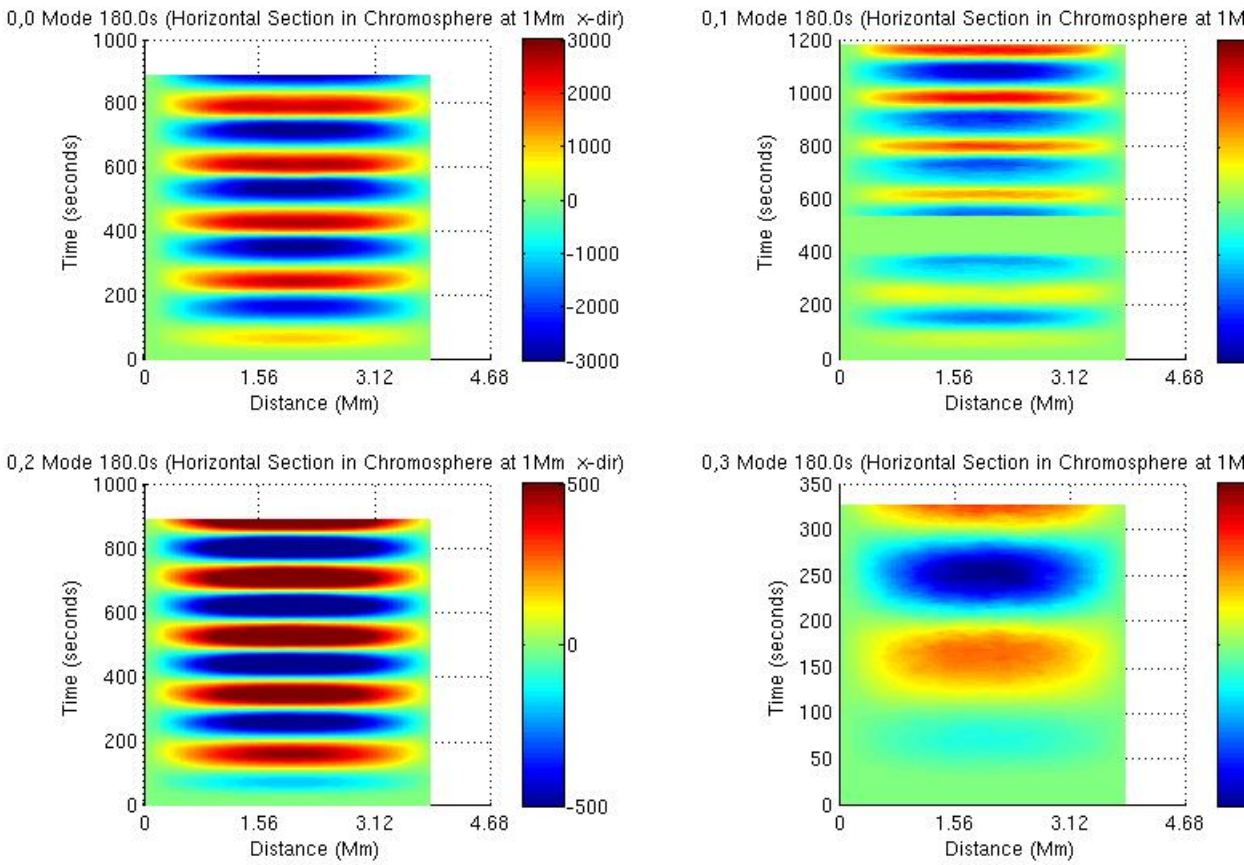

Figure 15: Distance time plot for modes with 180s period Horizontal Section through the Chromosphere (at 1Mm) for the z component of the velocity. x-direction

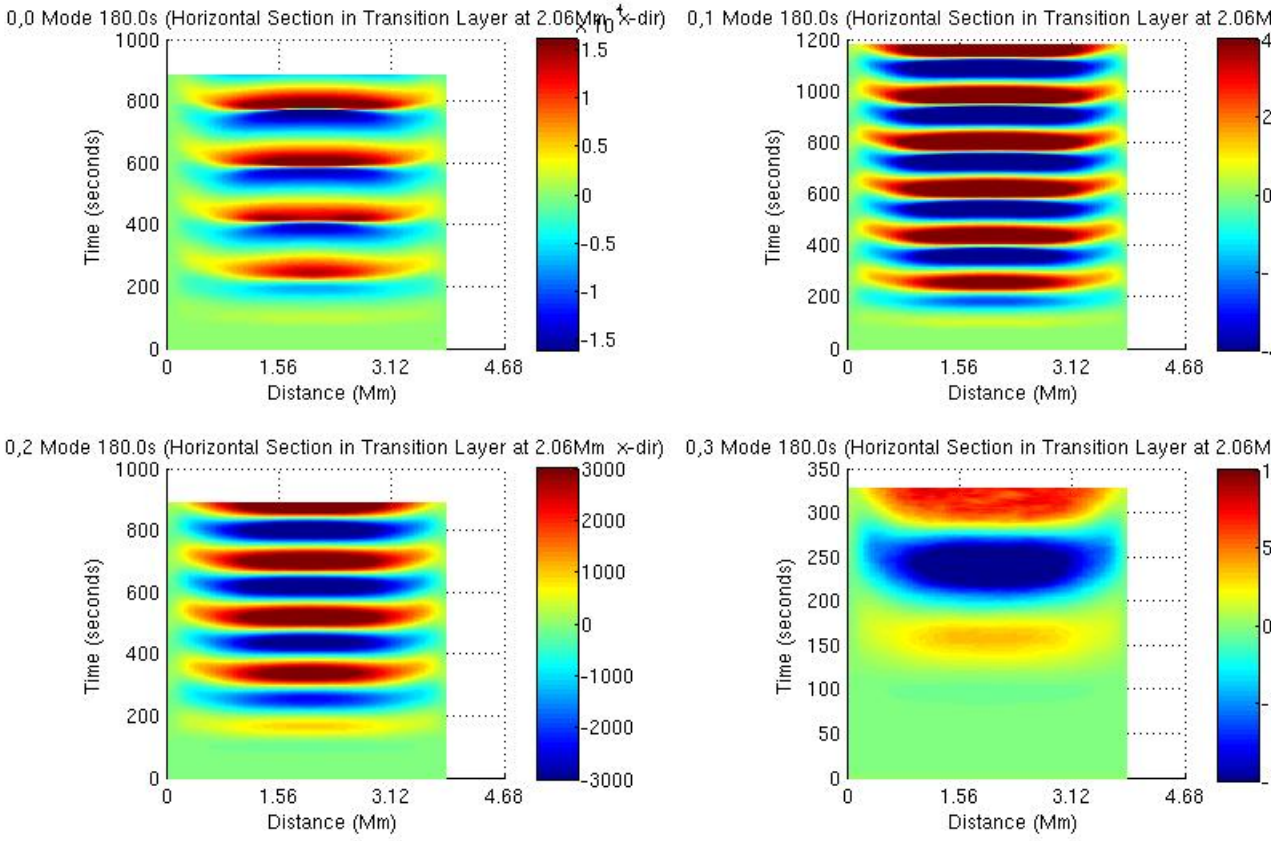

Figure 16: Distance time plot for modes with 180s period Horizontal Section through the Transition Region (at 2.06Mm) for the z component of the velocity. x-direction

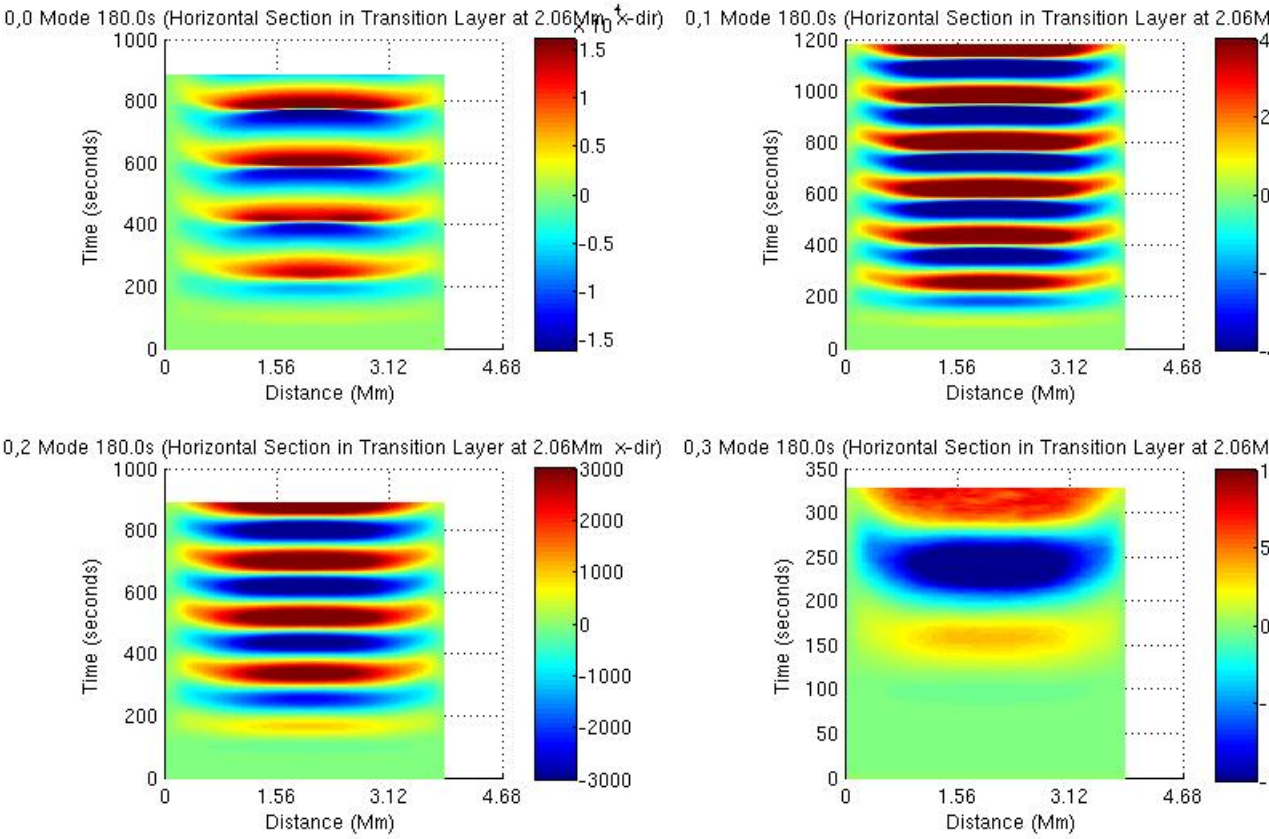

Figure 17: Distance time plot for modes with 180s period Horizontal Section through the Solar Corona (at 4.3Mm) for the z component of the velocity. x-direction

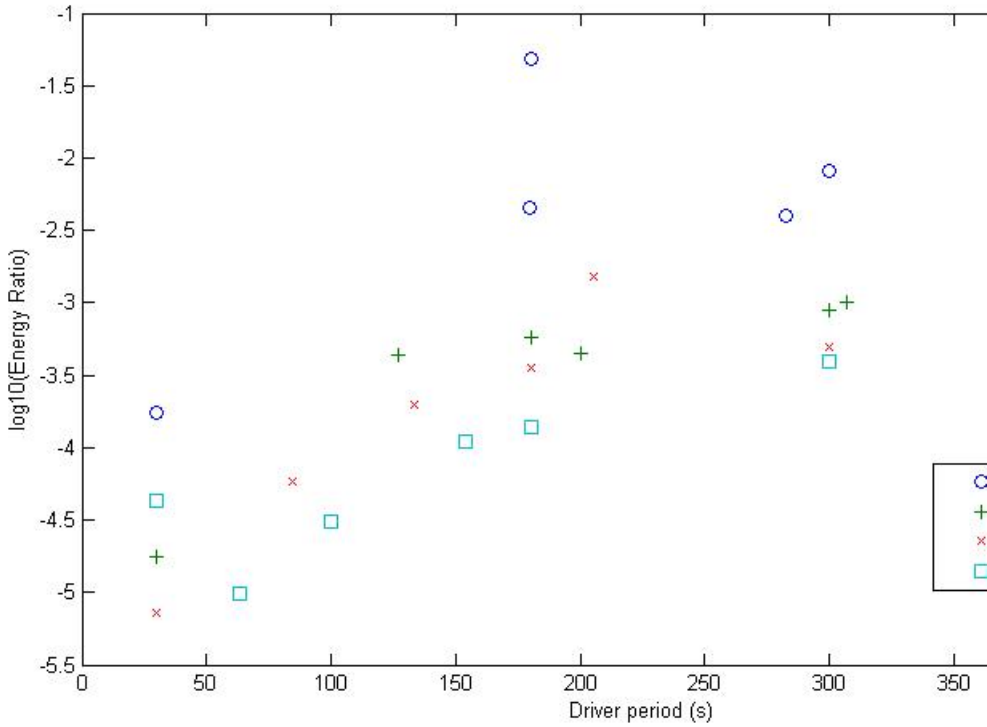

modes$_5$p5$Mm.jpg$

Figure 18: Variation of Energy Flux Ratio with the Driver Energy at a Height of 5.5Mm for a Solar Atmosphere Excited with a p-Mode Driver Located at a Height of 100km

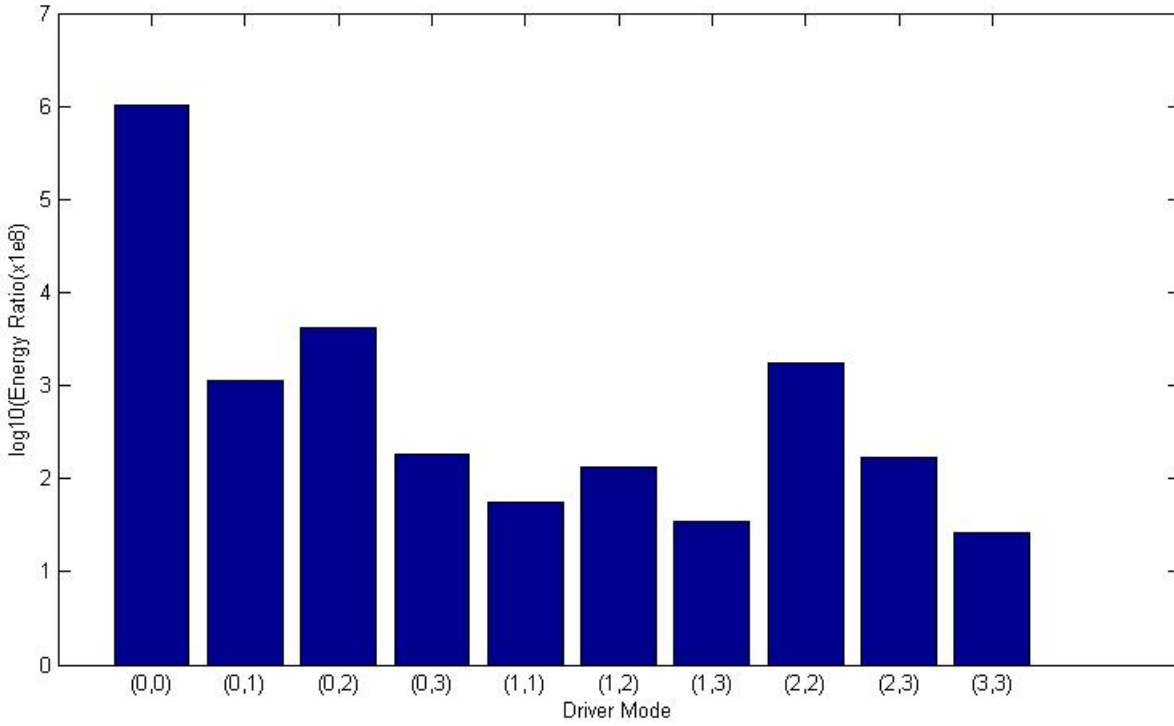

Figure 19: Variation of Energy Flux Ratio at a Height of 5.5Mm for a Solar Atmosphere Excited with a 180s p-Mode Driver Located at a Height of 100km

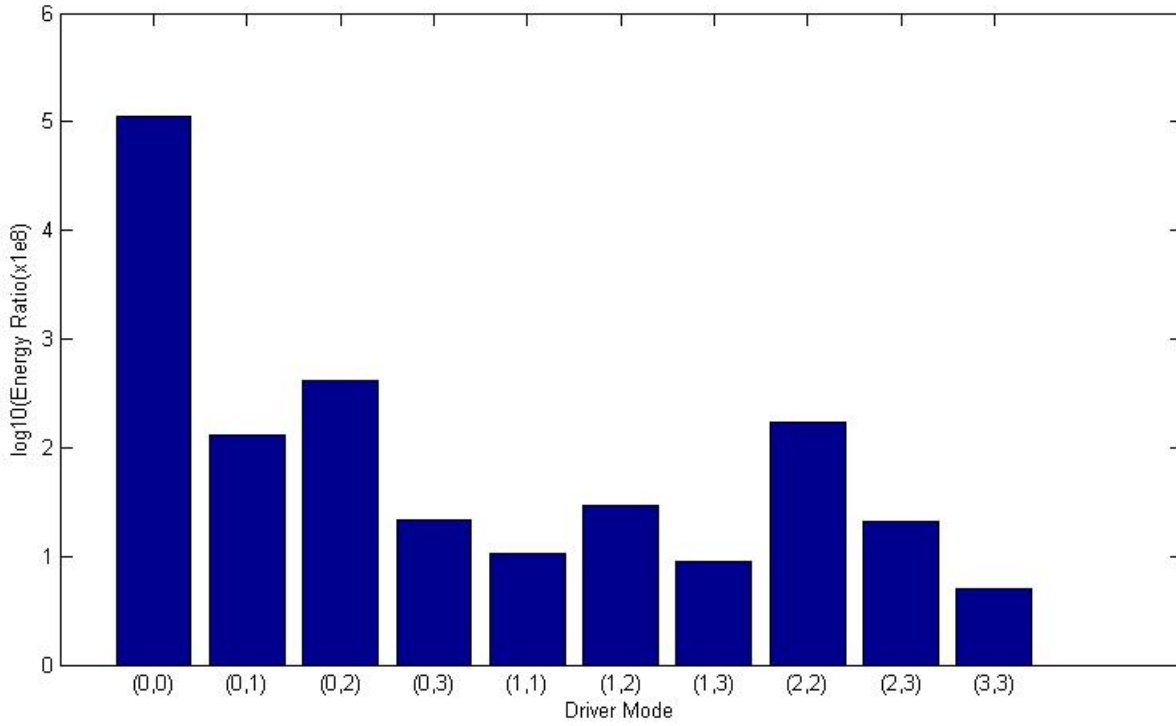

Figure 20: Variation of Energy Flux Ratio at a Height of 5.5Mm for a Solar Atmosphere Excited with a 300s p-Mode Driver Located at a Height of 100km

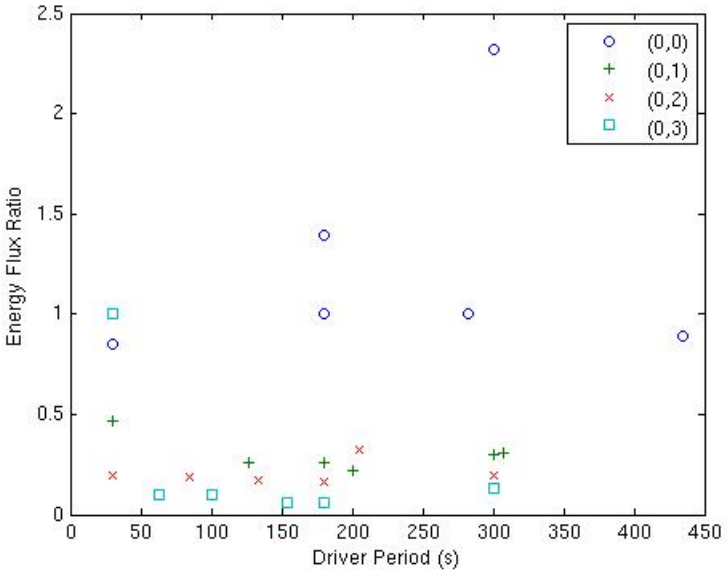

modes$_5$p5$Mm.jpg$

Figure 21: Variation of Energy Flux Ratio at a Height of 5.5Mm for a Solar Atmosphere Excited with a p-Mode Driver Located at a Height of 100km